Gasification of in-Forest Biomass Residues

Kenneth B Faires

A dissertation submitted in partial fulfillment of

the requirements for the degree of

Doctor of Philosophy

University of Washington

2013

Reading Committee:

Daniel T. Schwartz, Chair,

Per Reinhall, Co-Chair,

John Kramlich,

Program Authorized to Offer Degree:

Mechanical Engineering

Kenneth B Faires

University of Washington

Abstract

Gasification of in-Forest Biomass Residues

Kenneth B Faires

Chair of the Supervisory Committee
Daniel T. Schwartz, Committee Chair, Chemical Engineering
Per Reinhall, Co-Chair, Mechanical Engineering

Described is a laboratory-scale continuous-feed supercritical water gasification (SCWG) system. The system is operated using real-world Ponderosa Pine sawmill residues at high biomass loadings, short mean residence times (2-5 sec), and 27.7 MPa pressures. Each run with the SCWG system typically processed several 100 g of biomass/water slurry mixture. We evaluated the effect of operating temperatures (from 700K to 900K) and biomass feedstock loadings (5% to 15% by weight in water) on solids conversion and gaseous product composition. Biomass-to-gasified product conversion efficiencies ranged from 89% to 99%, by mass. Gaseous products were primarily composed of CO_2, H_2, CH_4, and CO, generally in that order of prevalence. The highest hydrogen yield, 43% mole percent, was achieved at 900k with a 5% biomass loading. In general, low biomass loadings corresponded to higher H_2:CO_2 ratios, but never did we observe stoichiometries that could be explained purely by steam reforming or steam reforming plus water gas shift chemistries. Methanation & Hydrogenation chemistry also occurred, but the mole fraction of CH_4 never exceeded 10%. We hypothesize that the real-world biomass samples used here intrinsically include gas-bubbles in the slurry, enabling partial or complete oxidation to occur along with the more conventional SCWG chemistries. As a result, the observed syngas composition was shown to depend more on biomass loading than on processing temperature. In-situ Raman testing was also evaluated as a possible means of monitoring SCWG real time. Biomass (lignin, cellulose, and hemicellulose) were all detected along with variations in concentration. Additionally effluent composition was verified to not contain intermediary compounds.

Table of Contents

CH1: Introduction

1.1 Residual Biomass

Despite advances in the technologies used to extract fossil resources, their reserves are finite, meaning production will peak and then eventually fall. Current predictions of peak oil production suggest that global supply will begin to decline between 2010 and 2030 [SOR12]. Biomass-derived fuels are among the most promising approaches for partially addressing to the problem of decreasing fossil fuel supply. Biomass is a large renewable resource, and when sourced from agriculture and forestry residues, construction and demolition wastes, and ecological restoration (such as fuel treatments), it does not compete with food production and is among the most ecologically sound bioenergy resources [SEA08].

Several studies have speculated that petroleum use could be greatly reduced, if not eliminated altogether, if biomass was properly used [EIA12, PER05,& NAT05]. The net consumption of crude oil per day in the US is 19,148,000 barrels [EIA12]. This is equivalent to more than 100 petajoules per year. This level of consumption could be met with currently available biomass, according to some estimates. Table 1.1.1 shows a widely cited estimate of the available amounts of biomass within the US, all of which are applicable to use for pyrolysis and SCW gasification (the technologies studied here) [PER05].

Feedstock	Bone Dry Tons (BDT)
Logging & Other Residue	64,000,000
Fuel Treatment	60,000,000
Urban Wood Residues	47,000,000
Wood Processing	70,000,000
Pulping Liquors	74,000,000
Fuel wood	52,000,000
Agricultural Residue	284,000,000
TOTAL (with moderate agricultural increase)	**651,000,000**

Table 1.1.1: Available Biomass Within the US (of Applicable Types/yr) [PER05]

Nominally, biomass has an energy content of 12-18 MJ/kg. If one solely compares available biomass to that of petroleum used (on an energy basis) the net available energy from biomass is 7100 petajoules. If one takes into account these two numbers it is obvious that biomass has significant potential as an energy offset. While the technology and infrastructure for such a drastic change has not yet been brought into being, it is our goal to explore novel engineering approaches for supporting the use of this resource to the benefit of society.

At the same time, excess biomass can be an ecological problem for land managers. For example, over the past century, policies that aggressively excluded fire from forest lands has allowed our forests to suffer from an 'epidemic of trees' [HES09]. Restoration of over stocked forests is now being carried out to arrest this 'epidemic' and return resilience to the landscape [HES09]. This so-called fuels reduction effort generates large quantities of waste biomass residue [PER05 & POL07]. Furthermore, current timber harvesting practices produce a significant amount of waste biomass residue that must be disposed. Burning this biomass residue on site is generally the most cost effective means of removal. This means of disposal, though inexpensive, does not make use of the biomass as an energy resource and suffers from severe limitations such as air quality impacts and wildfire potential during the burn. As such, the need to find alternative methods and techniques to allow excess biomass to be removed from the forest while making use of it as a resource is increasingly important. Not only does removal improve the overall health of a forest, but vital habitats can be restored, along with increased fire resiliency and resistance to insects/disease [HES09 & POL07]. Intelligent removal of specific types and quantities of biomass is not only a source of sustainable energy, but also of vital importance to ensuring a stable environment for all of earth's inhabitants: plant, animal, and human alike [HES09].

The transport of biomass from remote parts of the forest to a centralized processing facility is an expensive and potentially cost prohibitive portion of the overall process required to make use of the energy content within the biomass [ERI08, HAM05, & PET08]. Strategies for reducing biomass transportation costs are sought to improve profit margins and increase the amount of economically accessible biomass [CUN08 & PET08]. This is especially important when considering forest restoration, which often requires the removal of unmerchantable timber [POL07]. A number of processes allow for a combined effect of reducing transportation costs while upgrading the biomass to a more merchantable product such as liquid fuels, synthesis gas, biochar, etc. [POL07 & SEA07]. These densification/conversion techniques can help reduce other handling and processing costs as well.

1.2 Super Critical Water Gasification

Several technologies are currently emerging for the purpose of converting biomass to energy and other value-added products. Gasification, one such technology, is the partial oxidation of biomass in order to convert it into the energy-rich and versatile form called syngas [MAT05]. This can then be used in fuel cells, diesel engines, or recombined to form larger hydrocarbons to serve as drop-in replacement fuels. Gasification is most often carried out in a reactor in which the fuel:air ratio is carefully controlled at about one-third of the stoichiometric value for complete combustion [WAN08]. Such systems can be classified on the basis of how the product gases are vented off and/or in regards to the method of heating the biomass. Primary products produced are carbon monoxide (CO) and hydrogen (H_2) although nitrogen (N_2) and carbon dioxide (CO_2) are also present in substantial quantities along with char and ash [WAN08]. Key issues include coking within the gasifier and contaminants in the resulting syngas (i.e., particulates, tars, alkali, nitrogen, and sulfur compounds) that limit or impact the performance of syngas in use [MAT05, YAN06, KRU08, KRU09].

Supercritical water gasification (SCWG) [MAT05, YAN07, KEL07, DIB07] promises to solve key issues for biomass gasification. In SCWG, the reactor is pressurized and the temperature balanced such that water within the biomass is at its critical point. The process is ideal for wet biomass containing as much as 99% water, eliminating the need to dry materials prior to processing and bringing the carbon build-up to <5%. SCWG has been demonstrated in the laboratory [YAN06, LU 07, HAO03] and in pilot applications [DIB07]. Initial work has begun to uncover the governing mechanisms for SCWG [YAN06, LU 07], but opportunities exist to advance the relationships between hardware design, feed composition, syngas quality, reliability, and system scalability.

The primary focus for SCWG research so far has been determining the scope of useable feedstocks and performance modeling. Within the context of feedstock evaluation, simplified biomass such as sugars (including glucose, cellulose and lignose) processed in batch reactors and/or quartz vials have been investigated by Hao, et al. and Matsumura, et al. [HAO03 & MAT05]. It was found that SCW effectively breaks down the base molecules of biomass into syngas consisting almost entirely of CO, CO_2, CH_4, and H_2 [HAO03 & MAT05]. Furthermore, it was found that the effect of reaction temperature on glucose gasification had a substantial impact [HAO03 & MAT05]. Hao determined that at temperatures of 923 K or higher 'complete' gasification can be achieved and the mass of the product gases can exceed the mass of the biomass feedstock due contributions from the breakdown of water [HAO03]. Glucose, cellulose, and lignose were all successfully converted to syngas utilizing the process [MAT05]. Overall, these prior results suggested that SCWG is a promising conversion process for biomass.

Yanik, et al. and Lu, et al. investigated SCWG of actual biomass, with a focus on product gases [YAN07 & LU 06]. Yanik, et al. tested a total of eight different types of biomass: tobacco stalk, corn stalk, cotton stalk, sunflower stalk, corn cob, oreganum stalk, chromium-tanned waste, and vegetable-tanned waste [YAN07]. Lu, et al. performed experimentation on wood

sawdust, rice straw, rice shell, wheat stalk, peanut shell, corn stalk, corn cob, and sorghum stalk [LU 06]. Both groups of experimenters successfully converted the biomass to gaseous products (CO, CO_2, H, and CH_4) [YAN07 & LU 06]. Lu, et al. also discovered small amounts of higher hydrocarbons, C_2H_4 and C_2H_6, in addition to the formation of oil-like tar observed on the surface of the aqueous solution [Lu 06]. Of note is the fact that Yanik, et al. utilized a tumbling batch autoclave, whereas Lu, et al. utilized a continuous feed tubular reactor [YAN07 & LU 06]. As such Lu, et al. was able to determine that hydrogen yield increases with increasing pressure, whereas methane and carbon monoxide show a decrease as pressures increase [Lu 06]. They also noted a decrease in carbon along with an increase in hydrogen and methane gases when process temperature was raised from 873 k to 923 k [Lu 06]. Increases in residence time yielded similar results; methane and hydrogen levels increased as residence time was increased from 9s to 46s [Lu 06]. Yanik, et al. utilized a batch process in which biomass was held at a fixed temperature/pressure for one hour. They were unable to determine the effects of variations in residence time, temperature, and/or pressure but were able to determine that successful conversion from biomass to syngas did occur [YAN07]. Of note were the variations in coking for different feedstocks. Yanik proposed that variations in feedstock lignin content was responsible, in part for the five-fold variation in coking [YAN07]. However, two feedstocks had identical lignin content, but showed a two-fold variation in coking, leading to the conclusion that not only lignin amount, but structure can influence coking within the system [YAN07]. There were also indications that organic materials other than cellulose, hemicelluloses, and lignin may have effects on syngas composition and coking [YAN07]. Yanik, et al. was able to analyze the waste water left over from the gasification process and discovered the presence of acetic acid, formic acid, furfural, and phenol residues.

Di Blasia, et al. investigated the use of SCW to remove tar/waste created from an updraft gasifier (water content >90%) [DIB07]. The primary purpose of the experimentation

performed by Di Blasia, et al. was to determine if it was possible/feasible to use SCW as a clean-up process for tar created from pyrolysis type reactions [DIB07]. The actual test specimens were gathered downstream of an updraft wood gasification plant [DIB07]. Organic compound levels of 6.5-31 g/l were observed, and SCWG converted between 30% and 70% of the material [DIB07]. The test specimens contained a total of 23 tar compounds [DIB07]. Sugars and complex phenols were quickly converted while intermediate products, such as furfurals, were slower to decompose [DIB07]. Residence times between 46-114 seconds at temperatures of 723-821 K were used with trend analysis showing that higher temperatures and increased residence times improve the amount of product gases [DIB07]. Overall the experimentation successfully demonstrates the use of SCW as a means of conversion/clean-up for liquid effluents generated from other forms of biomass gasification [DIB07].

Describing the governing chemical reactions and thermodynamics for SCWG is an important element in understanding the performance and products of a system [KEL07, YAN06, LU 07]. Though biomass in and of itself can vary greatly, generally all biomass can be represented by $C_xH_yO_z$ (e.g., glucose is $C_6H_{12}O_6$ and cellulose is a polymers of glucose) [HAO03]. While biomass always has some absorbed minerals and other contaminants, the simple representation $C_xH_yO_z$ is a suitable descriptor for the majority of biomass components (cellulose, hemicellulose and lignin). The simplest chemical description of SCWG of biomass is [KEL07]:

$$\text{Biomass} + H_2O \rightarrow CO + H_2$$

$$CO + 3H_2 \rightarrow CH_4 + H_2O$$

$$CO + H_2O \rightarrow CO_2 + H_2.$$

The first reaction is known as steam reforming, in which the biomass is broken down into carbon monoxide and hydrogen [KEL07, HAO03, YAN06]. The second reaction, methanation, is the

result of the combination of ambient hydrogen and carbon monoxide [KEL07, HAO03, YAN06]. The third reaction is considered a water gas shift reaction and results from a breakdown of the water [KEL07, HAO03, YAN06]. It is believed that temperature and pressure within the system determines which of the three reactions will be dominant [LU06]. Higher temperatures and pressures favor hydrogen production, while lower ones tend to favor methane production [LU 06]. Temperatures can range from 650k to 1000k with pressures on the order of 20-35MPa, although typical temperatures are 700-800k at pressures near 25 MPa [HAO03, YAN06, GUO07].

Residence time studies by Lu, et al. show H_2 & CH_4 levels increase as residence time increases (9-46s) [LU 06]. The primary purpose of their studies was to focus on the parametric effects within the process. Various forms of biomass were pretreated and mixed in order to obtain a uniform mixture of 2 %(w/w) biomass combined with 2 %(w/w) sodium carboxymethylcellulose in order to facilitate feeding within the system [LU 06]. Of additional importance is the fact that they pre-ground the biomass to 40 mesh prior to mixing [LU06]. Their experimentation showed that not only did higher residence times result in an increased yield of hydrogen, but increased pressure and increased temperature result in improved hydrogen output as well [LU 06]. One should note that of the two temperatures tested, 873 K and 923 K, higher temperatures resulted not only in improvement of hydrogen production, but also in the overall carbon efficiency and net production of all product gases [LU 06]. This is in contrast to increasing pressure which had the effect of increasing the hydrogen content while decreasing levels of CH_4 and CO [LU 06].

Another important aspect of research in SCW is potential catalyst action from the machines involved in the actual processing. The important aspect of this type of research is to try to separate the effects of SCW versus the combined effect caused by metals in combination with SCW [RES07, RES08, RES09, & RES10]. Common ideas theorize that platinum,

ruthenium, rhenium, and nickel are among the major metal catalysts in SCW gasification of biomass [RES07, RES08, RES09, & RES10]. In order to determine their effects a series of experiments were carried out in quartz batch reactors by Resende, et al. These experiments not only showed the synergistic effects of reactor materials with SCW's properties, but also attempted to delve further into the nature of the reactions that were occurring. The following reaction pathway was developed to better understand the detailed steps involved in SCWG of biomass:

Lignin Hydrolysis	$(C_{10}H_{10}O_3)_n + nH_2O \rightarrow nC_{10}H_{12}O_4$	(1)
Monomer Oligomerization	$nC_{10}H_{12}O_4 \rightarrow (C_{10}H_{10}O_3)_2 + (C_{10}H_{10}O_3)_3 + \ldots$	(2)
Monomer Decomposition:	$C_{10}H_{12}O_4 \rightarrow C_xH_yO_z$	(3)
Steam Reforming I:	$C_xH_yO_z + (x\text{-}z)H_2O \rightarrow xCO + (x\text{-}z + y/2)H_2$	(4)
Steam Reforming 2:	$C_xH_yO_z + (2x\text{-}z)H_2O \rightarrow xCO_2 + (2x\text{-}z + y/2)H_2$	(5)
Char Formation:	$C_xH_yO_z \rightarrow wC + C_{x\text{-}w}H_yO_z$	(6)
Water-gas Shift:	$CO + H_2O \rightarrow CO_2 + H_2$	(7)
Methanation:	$CO + 3H_2 \rightarrow CH_4 + H_2O$	(8)
Hydrogenation:	$CO + 2H_2 \rightarrow CH_4 + 1/2O_2$	(9)

This more complete set of reaction expressions is especially valuable for interpreting how SCWG process variables modify the product selectivity and yield. Resende, et al. showed clearly that metal reactors had a significant effect on the quantity of gases produced [RES07, RES08, RES09, & RES10]. While no detrimental effects were discovered, it highlights the fact that material selection is key in optimizing gas yields and brings to light a possible mechanism responsible for variation in yields, such as deactivation of catalytic surfaces [RES07, RES08,

RES09, & RES10]. This is vital information for understanding possible variations in data that may occur during extended testing. Resende, et al. carried out experiments in batch reactors and showed that SCWG could be achieved at high concentrations of biomass (33%) [RES07, RES08, RES09, & RES10]. This data is promising for metal continuous fed reactors, in that, it demonstrates that more favorable thermodynamic concentration may be pursued.

In summary, previous research has shown the validity of SCWG utilizing a series of steps progressing from constituents of biomass to actual biomass with very high water content and area-specific feedstocks. Furthermore, the process has been demonstrated effective in the treatment of waste water, illustrating its potential for use as a 'clean-up' method after various other processes. While the process offers a variety of advantages, such as removal of the need to dry biomass, there are some distinct challenges that continue to pose sizeable obstacles to further research and implementation of the process for large-scale industrial use.

Key obstacles for moving SCW from the realm of research to that of industrial use are: (1) reducing the water content required to carry/process the feedstock (thereby improving the energy balance whilst reducing preprocessing), (2) expanding data on the selection of feedstocks to include those locally available, and (3) developing viable continuous feed reactors in order to move away from batch reactions, thus increasing speed/volume of material processed. Of note is that continuous feed reactors are typically plagued by coking issues [GUO07].

The Pacific Northwest in particular could benefit significantly from industrial scale SCWG as this region suffers from a significant amount of residual biomass in the form of wood. This woody waste offers vast potential as an energy source if it can be utilized. To date there is not any data on SCW syngas produced from woody biomass species. This thesis research makes a significant contribution to meeting the need for such SCWG data and processes.

CH2: Summary of Research Objectives

2.1 Design & Build Supercritical Water Gasification System

Our first objective was to design and build the first continuous feed SCWG system capable of processing 'high' concentrations of woody biomass. No UW facility currently has a reactor; thus, a major component of this project was the design and construction of such a device. The majority of previous researchers have used simple batch reactors. Batch reactions are, however, not necessarily indicative of how feedstocks may react in a continuous reactor. Current research setups utilize commercially available pumps for pressurization. Because these pumps are typically not capable of moving multiphase media (solids+fluids) and/or withstanding the temperatures involved in SCW gasification of such media, only finely ground suspended particles (or dissolved sugars) with extremely high water content have been tested as feedstock. It was the goal of this research to reduce this barrier by testing a more representative feedstock/media.

2.2 Testing of SCW Gasified Ponderosa Pine

The objective of this experiment was to test Ponderosa Pine in a SCW reactor. The novelty of the test comes not only from the woody feedstock being processed in a continuous feed reactor, but also the extremely high concentration of biomass used here as compared to previous research [MAT05]. Ponderosa Pine was processed with biomass concentrations of 5x, 10x, 15x the levels of typical previous continuous feed reactors (1% by mass) [MAT05]. This was performed through a temperature range of 700-900K in 100 degree increments. The mass of the water/gas output was monitored 'real-time' via a Metler Toledo scale. A knockout drum was then vented into a GC for analysis. The residual mass of water was also weighed in order to close the loop on the mass balance. Electrical energy input into the system was also measured and recorded.

2.3 Evaluate Raman Spectroscopy for Use in Syngas Produced by SCW Gasification

Here we performed real-time optical diagnostics that have the capability of process control, an important aspect of any commercial technology. Gas Chromatography is the current means most researchers use to analyze the syngas produced. This requires samples to be drawn, moisture content managed, and measurements taken. The whole process can take several minutes. In contrast, Raman Spectroscopy offers a tool by which to potentially measure syngas as it is created within the reactor in near real time. It is one of the only technologies capable of withstanding the extreme temperatures and pressures involved in SCWG, with measurements taking seconds instead of minutes. Furthermore, Raman offers the ability to detect solids, liquids, and gases. This offers significant advancement in that the decomposition of biomass into syngas occurs via an unknown route. At best researchers have performed batch reactions in quartz capillaries and been able to visually observe the process [SMI09]. The process for conducting this investigation was to introduce a Raman probe into the SCW system during feedstock processing and compare results from the aforementioned Ponderosa Pine experiment, thereby validating (or disproving) the possible use of this technique in a SCW system. Real time gas stream analysis will allow near complete control over the output syngas making it ideal for the predictable production of hydrocarbons from biomass.

CH3: Approach to Achieve The Objectives

3.1 Design & Build Supercritical Water Gasification System

The creation of a SCW environment can be envisioned as a series of sub-steps. If one abstracts SCW into a simple definition of water that is at very high pressure and temperature, a designer can see that the key aspects are pressurization and heating whilst ensuring the flow of material through the system. As such the system was broken into a series of subsections that fed, pressurized, and then heated biomass. Figure 3.1.1 illustrates the basic process flow diagram for our continuously fed apparatus. The gasifier system consists of two vertical feed

tubes that hold the biomass slurry. The feed tubes alternately load a pair of piston/cylinders that are used to raise the slurry pressure to a level needed to achieve supercritical conditions. One achieves continuous high pressure flow to from the paired cylinder/feed system via a y-coupler and check-valve system. The reactor section is where the mixture is brought to supercritical temperatures. The reactor, made of 304 stainless steel, was heated with a series of four nichrome radiative heating elements with voltage controllers and operated at temperatures between 700 and 900 K. The reactor volume was 32 ml, and it was estimated that slurries reached supercritical conditions within the first few millimeters of entering the reactor. A backpressure throttle valve downstream of the reactor was used to maintain pressure in the reactors at 27.2 MPa, whereas flow rate (and hence residence time in the reaction zone) was controlled with a needle valve on the reactor exit via educing a choked flow condition. Pressurized product syngas was directed to a dead-end knockout drum where the liquid and gas were separated for subsequent analysis. For simplicity in this laboratory scale system, all waste heat from the product stream was dumped to the surroundings rather than thermally integrated with feedstock preheating. The knockout drum was stored at room temperature until analysis. Our biomass slurry flow rates (and hence residence times in the tubular reactor) were set between 1 and 5 gram/second with the needle valve.

Because of the high biomass loadings (5 to 15% by mass) and use of a needle valve, the flow sometimes displayed a slug-like behavior as it passed through the valve and into the reactor. To improve this at high solid loading, the 10% and 15% used 20 or 40 mesh sieved biomass. While higher levels of processing to produce finer biomass could further improve flow, we sought to test samples with minimal preparation. Table 7.6.1 in the Appendix annotates the particle size and approximate flow rates through the device. All product streams represent cumulative product acquired in the knockout drum over a long averaging time compared to this slug-like variation.

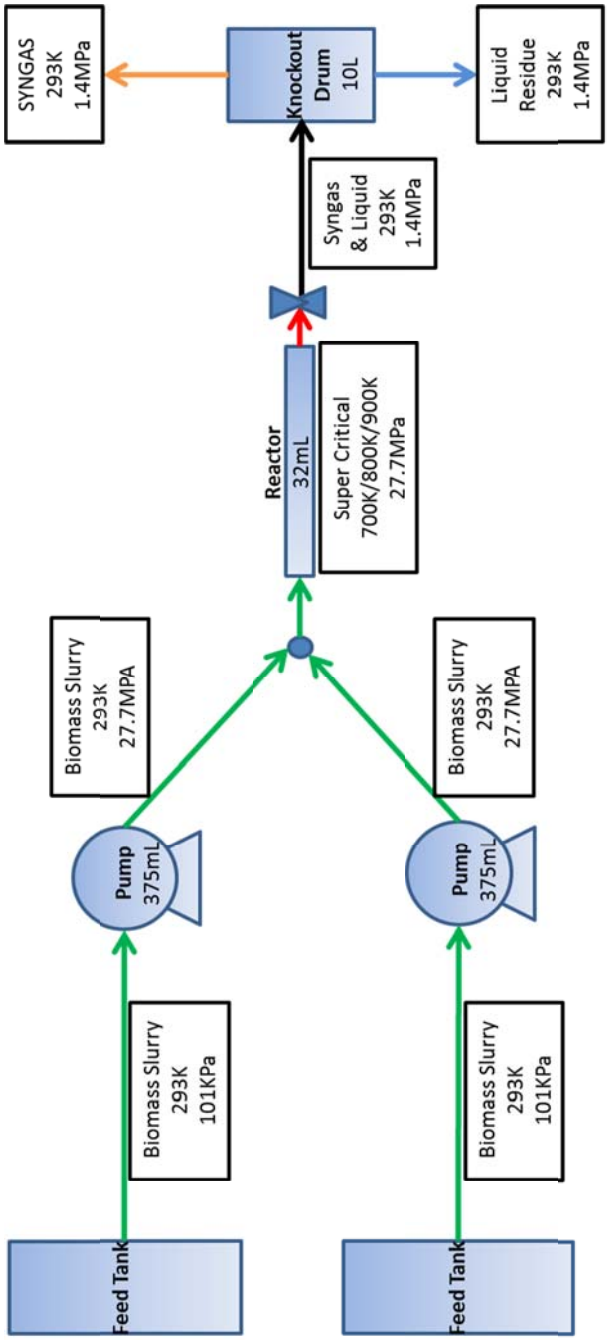

Figure 3.1.1: Process flow diagram for SCW system. Green arrows annotate feed with each box representing a mechanical system component

Before experimentation was allowed to begin the author was required to build a safety enclosure for the experiment. This was due to budgeting and the lack of an existing

containment area suitable for containing an explosion should the experiment go wrong. Due to shop limitations the entire enclosure had to be hand-fabricated in the lab. The design of the enclosure was centered on dampening shockwaves and containing debris that might result from a reactor explosion. The front panels of the enclosure were constructed of 5/16 inch polycarbonate. These were trimmed with ¼ " by 2" aluminum bar stock in order to provide additional stiffness and a means by which to mount the panels. Additional energy absorption was provided by placing shear pins along the edges of the polycarbonate. In the event of an explosion the deflection of the panels would transfer into the aluminum trim and result in pin failure. The framing of the enclosure was constructed of over 150 feet of 2 inch x 1/8 inch angle iron. Mild steel was chosen due to its flexibility in an attempt to add further means of absorbing energy without fracture. The top, back, and side were sheeted in 22 gauge sheet metal with the bottom 2 feet being left open to vent any gases. The final product is depicted in Figure 3.1.2 below.

Figure 3.1.2: Safety Enclosure

The next consideration was the design of the gasifier. From the conceptual design phase it was decided that a reciprocating piston design would be used. A number of actuation

methods were looked at, but in the end, a hydraulic ram assembly was decided upon. This was due to the anticipated low cycle time between pistons, the need to reduce costs, and the desire to maintain simplicity. A key obstacle to utilizing hydraulic actuation was the extreme force that would need to be withstood in order for the system to work. A second, but equally important obstacle was the difficulty of maintaining system alignment throughout the assembly's length (necessary for a piston to properly seal in its parent cylinder).

The pump section was to be comprised of nominal 2 inch diameter cylinders. In order to pressurize these to the design pressure of 5,000psi the frame would have to withstand 7.7 tons of force per cylinder (force = pressure x area). If both pistons were actuated simultaneously the resultant force would exceed 15 tons. It was also desired that the entire system be portable and have a high safety factor. The end result was a skid type design comprised of two halves linked by cross members. By designing the frame in two pieces it made assembly of the system simpler in addition to making the frame portable by hand. In order for this approach to be used, the forces from the rams had to be transferred along a single axis lest the cross member prove insufficient. Mild steel push-blocks were used for this purpose. Mounting one block at the rear to the rams and another to the front end of the piston/cylinder assembly allowed for forces to be distributed into the larger, load-carrying members while avoiding any cross loading.

System alignment is vital for the proper operation of a piston-cylinder system. A major drawback of the pump section was the need for relatively long pieces and extremely high tolerances. The tolerance requirement was dictate by the O-ring gland design, with an end result of 0.00025 inches of radial interference. This had to be maintained along the 18 inch hydraulic rams throughout their entire 12 inch stroke. Furthermore, since the entire gasifier was designed and built with basic machinery donated to UW, a relatively high amount of discrepancy between the two piston sections could exist. In the end a free floating design was decided upon so that the gasifier could float between the piston connecting pins and the front end of the

piston/cylinder assembly. Macroscopic alignment was achieved via placing the cross members onto threaded rod so that they could be raised/lowered vertically. Because the frame was constructed in two halves with multiple cross members, such a setup allowed for adjustments in roll, pitch, and yaw of the components. In order to prevent the gasifier from dislodging, cross members were made in vertically opposing pairs; once the machine was aligned these could be tightened against each other, clamping the machine between them. When assembled the entire device can be lifted as a skid, or broken into four main subsections and hand carried. A single section is shown below in Figure 3.1.3.

Figure 3.1.3: Gasifier Frame Assembly

The pump section, shown below in Figure 3.1.4, is one of the key components of the gasifier. The designed operating pressure was set as 5000psi. Furthermore, the entire assembly was designed to withstand extremely high heat and thermal gradients so that the pump could be directly in contact with the reactor. This meant that one end of the assembly could be exposed to temperatures as high as 1000^{o} C while the other end would be operating at near ambient temperatures. Due to the necessity of maintaining extremely tight tolerances for sealing purposes, materials needed to have matched thermal coefficients of expansion; this was most easily achieved by using the same material throughout the working sections of the gasifier. Aside from the necessity of maintaining tolerances there was also the requirement that the corrosive properties of SCW be accounted for as well. Stainless steel is comprised of nickel and/or chromium mixtures with iron. Both alloying agents can have oxide layers that become

unstable in SCW applications [KRI04]. Oxygen levels, salts, and other chemical compounds all affect this and can result in component failure [KRI04]. Taking these factors into account it was decided to use 304 stainless. Through the course of machine testing it was discovered that severe galling occurred between the piston/cylinder interface; a change to a self-lubricating material with matched thermal coefficients was required for this particular component. Bronze (SAE 660) was satisfactorily tested and is currently being used as the piston material.

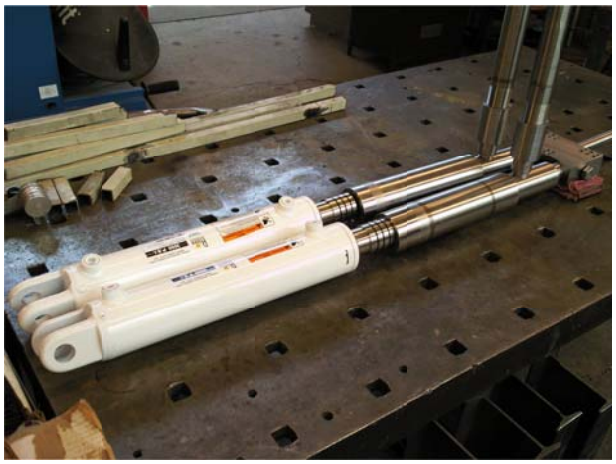

Figure 3.1.4: Pump Assembly

Pistons for the system needed to be both self-aligning and matched thermally with the remainder of the system. An O-ring was chosen for sealing due to high system pressure. A set of three Aflas O-rings were affixed to each piston. In order to prevent leakage the interface was designed such that any single O-ring would be able to seal system pressure. Aflas was the chosen material due to its resistance to aggressive media and its compatibility with pulp and paper liquors. A straight piston with a beveled edge was used initially in order to minimize particle accumulation between the piston and cylinder. After several hours of operation, severe galling (from misalignment) was found within the cylinders ultimately resulting in system failure. A hemispherical piston design was attempted in response to this initial failure. A significant level of improvement was found with this design; however, system failure due to galling still

occurred. Eventually a bronze material was found that thermally matched the stainless steel cylinders and offered the advantage of being self-lubricating. A set of pistons incorporating the new material and hemispherical design were constructed and installed. No further issues have occurred and the system has operated without any signs of galling or mechanical wear.

To date coking has been a major issue in SCW gasification of biomass and often leads to system failure within hours [MAT05]. Coking results from biomass being exposed to temperatures below the gasification range, but above the carbonization temperature [HAS07]. Typically this range begins around 200^{o}C and continues up to the super critical range where gasification can occur [HAS07]. To address this issue, the author designed a y-coupler (Figure 3.1.5) for the reactor system that could function as an anti-coking technology. In order to maintain thermal control of the biomass, active cooling channels were built into the y-coupler of the system. This allowed the reactor section and the biomass it contained to be at super critical temperatures while ensuring that biomass upstream of the reactor remained below the coking range. Furthermore, the reactor was designed to have a significantly lower thermal mass than the y-coupler/pump sections. This design decision was based based on the concept that heat transfer has a limited number of drivers: temperature differential, transfer area, thermal conductivity, and net thermal energy. The temperature differential was set with respect to the coking limitation and SCW operating temperatures. It was desired to incorporate this feature while ensuring a high safety factor within the reactor. Leak-before-break criteria were used in order to ensure that critical crack propagation did not occur [DOW07]. For stress calculations cylindrical pressure vessel formulas were used [SHI01]. These are depicted below:

$$\sigma_{l-max} = \frac{pr_i^2}{r_o^2 - r_i^2} = \frac{5{,}000psi * 0.125_i^2}{0.5_o^2 - 0.125_i^2} = 333 \text{ psi}$$

$$\sigma_{t-max} = \frac{p(r_o^2 + r_i^2)}{r_o^2 - r_i^2} = \frac{5{,}000psi(0.5_o^2 + 0.125_i^2)}{0.5_o^2 - 0.125_i^2} = 5{,}670psi$$

This system is designed with a safety factor far in excess of the recommended 2:1 for reactor materials at temperature. Material properties such as thermal conductivity were considered in addition to reactor strength. Transfer area and net thermal energy could be configured in such a way as to prevent thermal leaching into other parts of the machine. A very small attachment area was used for the reactor section to the y coupler (Figure 3.1.5), thus limiting heat transfer upstream. The y-coupler and pump section were also constructed in such a manner as to contain significantly more material than the reactor. This design concept, called 'thermal mass', is one in which a system is thermally stabilized by manipulating the volume of materials within components. By having a reactor section of low mass (and equivalently low thermal mass) attached to a y-coupler/pump section that contained significantly more material (and resulting high thermal mass) heat transfer between the connection would not be sufficient to overheat the upstream components. This proved so effective in the design that active cooling proved unnecessary. The assembly is depicted below in Figure 3.1.6.

Figure 3.1.5: Y-Coupler

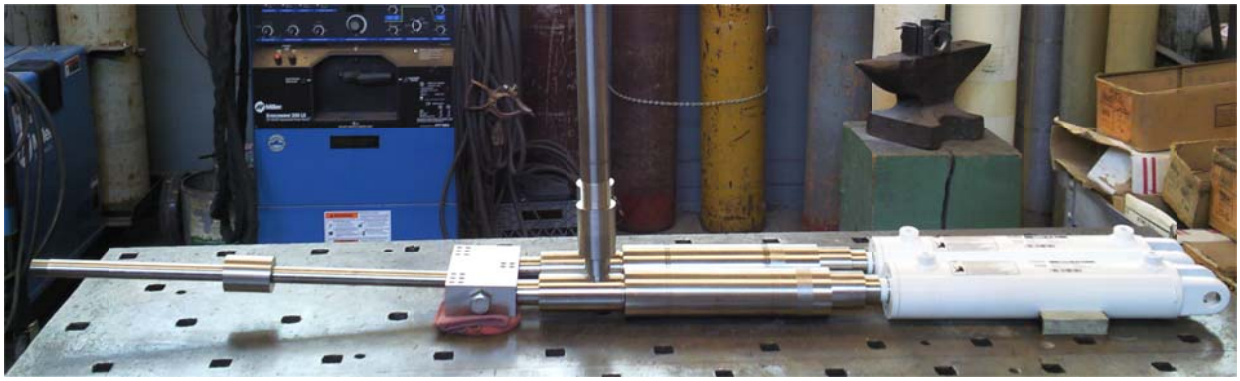

Figure 3.1.6: Gasifier Assembly Outside of Frame

Heating is achieved by four electric resistance coils controlled via voltage controllers. The entire electrical system is fed by a 3-phase 220V electrical distribution box. By powering the heating section electrically a simple amp meter can be combined with a volt meter to determine the input power for heating. Temperature is monitored via a thermocouple fixed to the mid-section of the reactor and shielded from the resistance coils. This section of the machine is insulated with ceramic insulation to minimize heat loss to the environment.

Pressure control upstream of the reactor is achieved via a bypass valve in the hydraulic actuation system as depicted below in Figure 3.1.7. This allows for pressure within the rams to be set. Because the force of the ram is directly proportional to this pressure (which is proportional to the pump pressure) the entire system pressure can easily be set. Downstream control is achieved via a pair of needle valves used to provide choked flow and maintain system pressure. Upon passing through the needle valves, system pressure drops to ambient where liquids and syngas separate within a knockout drum. The knockout drum sits on an industrial scale so that mass can be measured as it flows through the machine and into the drum.

Figure 3.1.7: System Hydraulic Controls

CH4: High solids continuous conversion of Ponderosa Pine w/ supercritical water

4.1 Background

Biomass-derived fuels are a promising approach for partially addressing projected declines in fossil energy supply ("peak oil") and restrictions on greenhouse gas emissions. Biomass is a large renewable resource that can impact a sizable fraction of the US demand [EIA12, PER05, & NAT05]. When sourced from agriculture and forestry residues, construction and demolition wastes, and ecological restoration projects (such as fuel treatments), it does not compete with food production and is among the most ecologically sound bioenergy resources [SEA08].

In a complex network of parallel and series reactions, as shown above, the careful selection of the reactor configuration and operating regime are critical for determining the product selectivity and yield [FOG05]. In order to achieve high throughput, SCWG will likely be operated as a continuous reactor rather than batch reactor. Continuous feed systems are much easier to operate at large scale, and they provide significant energy efficiency advantages

[MAT05, RES07, RES08, RES09, & RES10]. Most SCWG studies have used batch reactors, though one continuous SCWG of biomass has been previously described [LU06]. Research is needed to understand the performance of real-world feedstocks operated at high solid loading, especially in continuous feed systems. Due to the large energy input needed to create supercritical water, it is to keep biomass loading high.

Here we present a novel continuous flow SCWG reactor and evaluate the feedstock, Ponderosa Pine, at solid loadings an order of magnitude higher than prior work. Our studies offer new insight into the effect of how biomass to water ratios affects syngas production and provide new information on continuous feed system requirements. We seek to advance the understanding of relationships between hardware design, feed composition, syngas quality, reliability, and scalability.

4.2 Materials & Methods

Ponderosa Pine feedstock was obtained from an industrial saw mill directly from the production line (Figure 4.2.1). This feedstock was chosen due to its local availability and because it would allow for the testing of a real, modestly processed woody biomass resource. Samples were run with un-processed saw dust and ground biomass (20 and 40 mesh). The 20 mesh and 40 mesh samples are prepared using a Wiley mill via sequential grinding.

Figure 4.2.1: Ponderosa Pine Sawdust

Distilled water is added to the sawdust to achieve the compositions dictated in Table 4.2.2. The biomass/water slurry was allowed to sit overnight so that the wood was saturated.

Our biomass slurry flow rates (and hence residence times in the tubular reactor) are set between 1 and 5 gram/second with the needle valve. Because of the high biomass loadings (5 to 15% by mass) and use of a needle valve, the flow sometimes displays a slug-like behavior as it passes through the valve and into the reactor. To improve this at high solid loading, the 10% and 15% loading experiments used the 20 or 40 mesh sieved biomass. While higher levels of processing to produce finer biomass could further improve flow, we sought to test samples with minimal preparation. Variations in particle size within this range had no discernable effect on the syngas composition. All product streams represent cumulative product acquired in the knockout drum over a long averaging time compared to this slug-like variation.

For product gas analysis, an Agilent 3000 Micro Gas Chromatograph (GC) is used. For this research, the device is configured with two columns and a thermal conductivity detector. A MolSieve column is used to separate non-condensable gases and light hydrocarbons whereas a PLOT U column is used for hydrocarbons ranging from C1-C7 in addition to CO_2 and water. The detailed operating conditions for the GC are listed in Table 4.2.1:

Channel A	Channel B
MolSeive	Plot U
Backflush	Fixed Volume
Carrier Gas: Argon	Carrier Gas: Helium
Injection Temp: 90C	Injection Temp: 90C
Column Temp: 66C	Column Temp: 50C

Table 4.2.1: GC operating parameters

For the mixture of gases anticipated in syngas from SCW it was decided that Agilent's Refinery Gas Analyzer (RGA) calibration gas mixture gas would be used to calibrate the GC. Figure 4.2.2 shows the output from the RGA standard for the two columns in the GC; this standard was used regularly to ensure long-term calibration accuracy.

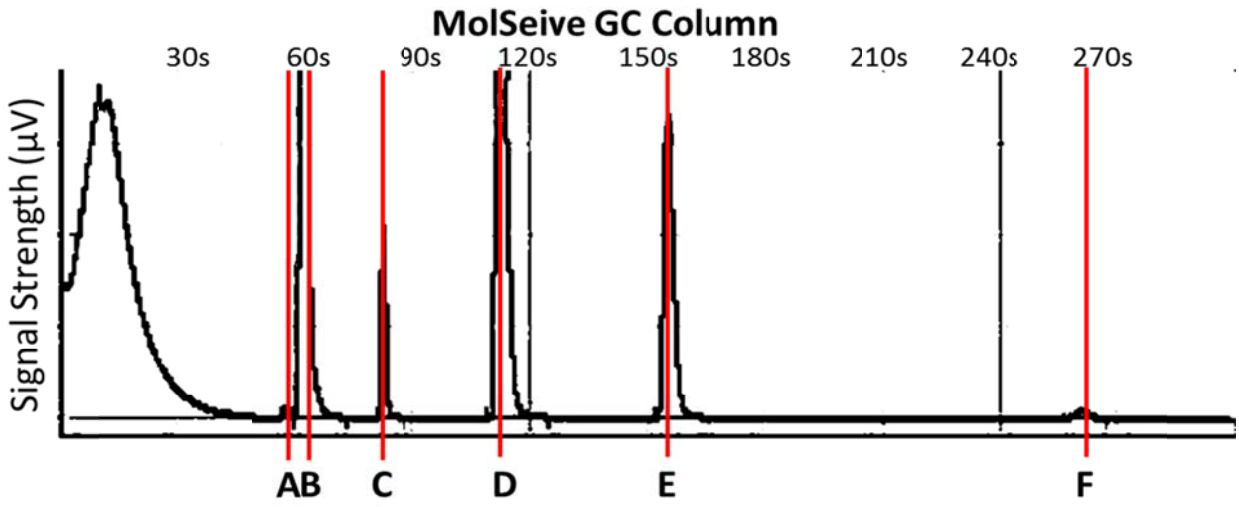

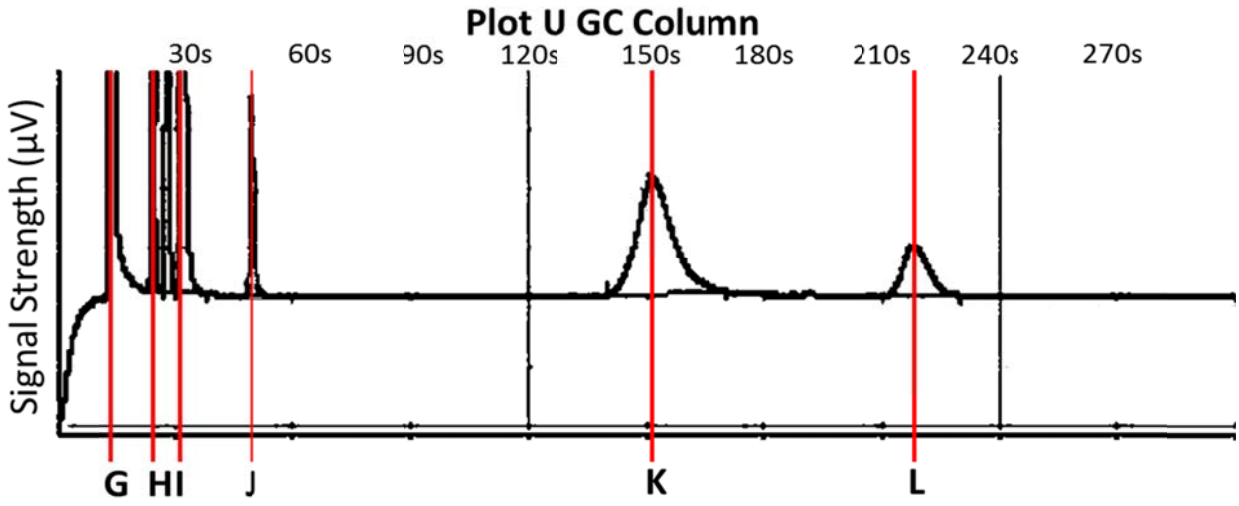

Figure 4.2.2: Annotated RGA standard gas calibration curve chromatograms. The labeled peaks correspond to gases contained within the standard, which includes all majar components in our syngas product chromatograms. The top chromatogram is from the MolSeive column while the lower chromatogram depicts the output from the Plot U column. Specific peak components include: A-Helium, B-Hydrogen, C-Oxygen, D-Nitrogen, E-Methane, F-Carbon Monoxide, G-Carbon Dioxide, H-Ethylene, I-Ethane, J-Acetylene, K-Propane, L- Methyl Acetylene]

Unknown concentrations for each component in our syngas product is determined through the linear proportionality of the area under the chromatogram peaks versus the concentration in the analyte. The peak area for a gas of unknown composition is compared to that of the known calibration gas peak area, producing a proportional gas composition. Figure 4.2.3 shows typical GC measurements made for syngas streams produced from SCW gasficiation of 90% water/10% Ponderosa Pine slurry.

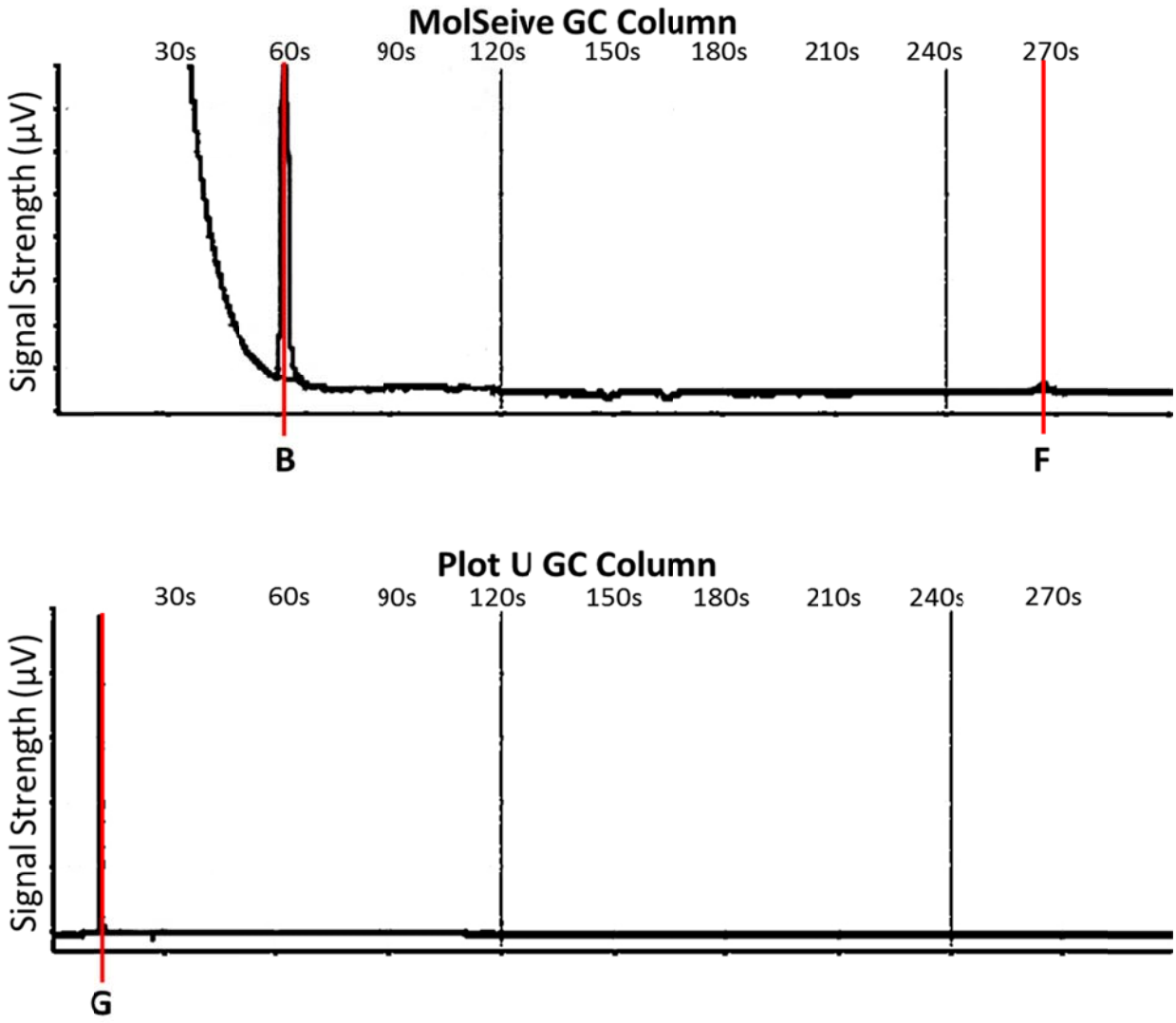

Figure 4.2.3: Typical syngas product stream chromatogram. The top chromatogram from the MolSeive column shows the presence of hydrogen (B) and carbon monoxide (F), while the lower chromatogram from the Plot U column shows carbon dioxide (G).

Research runs comparable to these were conducted at biomass concentrations of 5%, 10%, & 15% by mass. For each concentration, temperatures of 700, 800, and 900K were tested. Three replicate experimental runs are performed for each biomass sample and set of process conditions, and 5 separate GC runs are performed for the syngas produced by each replicate. Thus, we assess both the process run-to-run reproducibility as well as the analysis uncertainty.

.

5% Biomass	10% Biomass	15% Biomass
90gram biomass (dry weight)	180gram biomass (dry weight)	270gram biomass (dry weight)
1690 grams DI Water	1600 grams DI Water	1500 grams DI Water

Table 4.2.2: Biomass/Water Ratios for GC Experimentation

The condensed product in the knockout drum is analyzed for each set of processing parameters to get the feedstock conversion efficiency. The solids remaining in the condensed product are separated using a Buchner funnel, dried, and weighed. The mass of product solid is compared to the initial feedstock Ponderosa Pine dry mass to obtain the biomass conversion.

4.3 Results and Discussion

The major products of SCW gasification are non-condensable gases. Nonetheless, examination of the condensable products from the knockout drum (Figure 4.3.1) is useful for visually illustrating important features of the biomass conversion process. Column A of Fig. 4.3.1 shows the three original feedstocks, from 5% biomass (top) to 15% (bottom) biomass. At 5%, the solids settle, whereas the 15% solids feedstock has the consistency of peanut butter. Columns B-D show examples of the condensed product for each of the feedstock slurries after processing at progressively higher temperatures (Column B is 700 K, Column C is 800K, and D is 900K). The condensed product from the knockout drum readily separates into a solid fraction on the bottom of each sample tube and a supernatant liquid. The photographs qualitatively suggest that, under all conditions used here, the biomass is largely converted into gaseous products (given the reduction in solids content); we quantify this conversation later. Nonetheless, there is a great deal that can be learned from the images alone.

A slight discoloration is clearly present in the liquid supernatant of Columns B-D in Figure 4.3.1. The supernatant liquid is transparent, with no turbidity, meaning the color is from soluble species rather than suspended solids. The complex reaction network proposed by Resende (Eqs. 1-9) show the production of intermediate molecular weight lignin hydrolysates and carbohydrate-like decomposition products, both of which are likely to be partially or fully soluble. There are substantial supernatant color differences between the 5% sample and the 10% or 15% sample, but little change in color as a function of temperature (*cf.* Columns C-D for a given Biomass %). These observations suggest that biomass fraction is a larger driver for the formation of soluble products than is temperature under our conditions. Preliminary Raman spectroscopy measurements on the supernatant liquid (not shown) suggest that the concentrations of these soluble organic compounds are very dilute. In addition to the soluble organic compounds made via gasification, any soluble salts that enter with the biomass will also end up in the liquid supernatant stream. Though outside the scope of this study, detailed study of the supernatant may be warranted to understand how this dilute product stream composition changes with processing conditions. Though not a large fraction of the total biomass conversion products, soluble components in the water may impact water treatment or recycling as one considers process scale-up and cost.

In the bottom of each sample container are fine particles of biomass and higher molecular weight (i.e., insoluble) reaction products from reaction equation (2) or (7). We view all the solid products as “unconverted” biomass, even though much of it is likely to be high molecular weight reaction product or insoluble inorganic material that entered with the biomass stream. The solid fraction appears to be significant (by volume), especially in the high biomass concentration images of Fig. 4.3.1, but it actually comprised a small fraction of the total feedstock biomass by weight. In all cases studied, the filtered and weighed solids fraction in the product stream is 11% or less of the total dry solid added to the feedstock slurry. Overall, we

see a nominal biomass conversion efficiency of roughly 95% across all runs we performed. While biomass conversion is generally highest at higher temperatures, no process run was below 89% conversion of the biomass. In short, the lack of significant quantities of high molecular weight solids or intermediate molecular weight soluble fractions means that the preponderance of biomass entering the system (between 89% and 100%) are converted to non-condensable gases over the range of conditions used here.

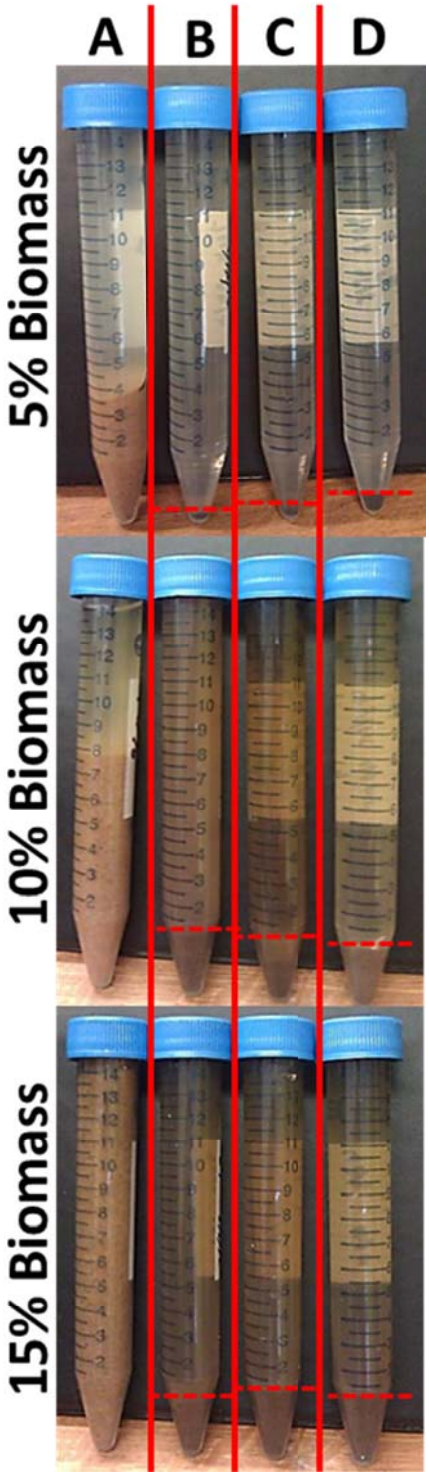

Figure 4.3.1: Examples of the liquid solution left over after processing. The effluent samples are arranged so that the left four are the 5% concentrations, the middle four are the 10% concentrations, and the last four are the 15% concentrations. Column A is unprocessed biomass, Column B is processed at 700K, Column C is processed at 800K, and Column D is processed at 900K

The syngas composition is shown in Figures 4.3.2A & 4.3.2B for the full range of conditions explored here. As noted in the Methods section, these data include both triplicate process runs (shown individually in Figure 4.3.2A, with each set of conditions demarked by vertical lines) and 5 separate samplings of the syngas for each run. Figure 4.3.2B combines the triplicate process runs into a single average data point in order to make trends more visible. The measurement order was randomized. The data show that errors associated with chromatography are small compared to run-to-run variations under nominally identical conditions, as expected (especially given the challenges of flow control for the viscous biomass slurries).

Figures 4.3.2A & 4.3.2B show that the expected four non-condensable gas species (H_2, CH_4, CO, and CO_2) were detected within each sample with the exception of the 700K & 900K runs at a 5% biomass loading in which CO and CH_4 were not detected. CO_2 is the dominant component, and hydrogen is second most prevalent in most cases. The concentration of CO can be appreciable, but CH_4 was never observed above a 10% molar fraction. Based on NIST thermodynamic data, the equilibrium coefficient (K_P) for the exothermic water gas shift reaction (Eq. 7) ranges from roughly $9.5 \geq K_P \geq 2.5$ over the temperature range of our experiments. Thermodynamically, this means water gas shift chemistry is always biased toward the products CO_2 and H_2, though at higher temperatures less so. In all cases, the high water activity during our reaction conditions strongly favors the production of CO_2 and H_2 via the water gas shift chemistry. Combining the fact that we have high biomass conversion and equilibrium chemistry favoring H_2 and CO_2, it is not surprising to see these as the dominant products. However, the fact that CO is present at molar fractions comparable to (or greater) than H_2 in several of the high biomass loading experiments, suggests there is more to the story. Kinetics, not just thermodynamics, may also play a role in our short residence time experiments. For example, previous research has been done with residence times as high as 75 minutes [RES07, RES08,

RES09, RES10] whereas the residence times used here are a few seconds. As we show below, plotting the data in Figures 4.3.2A & 4.3.2B in different ways helps illuminate thermodynamic and kinetic considerations for this system, as well as uncover the potential role of adventitious oxygen in these realistic high biomass feedstocks.

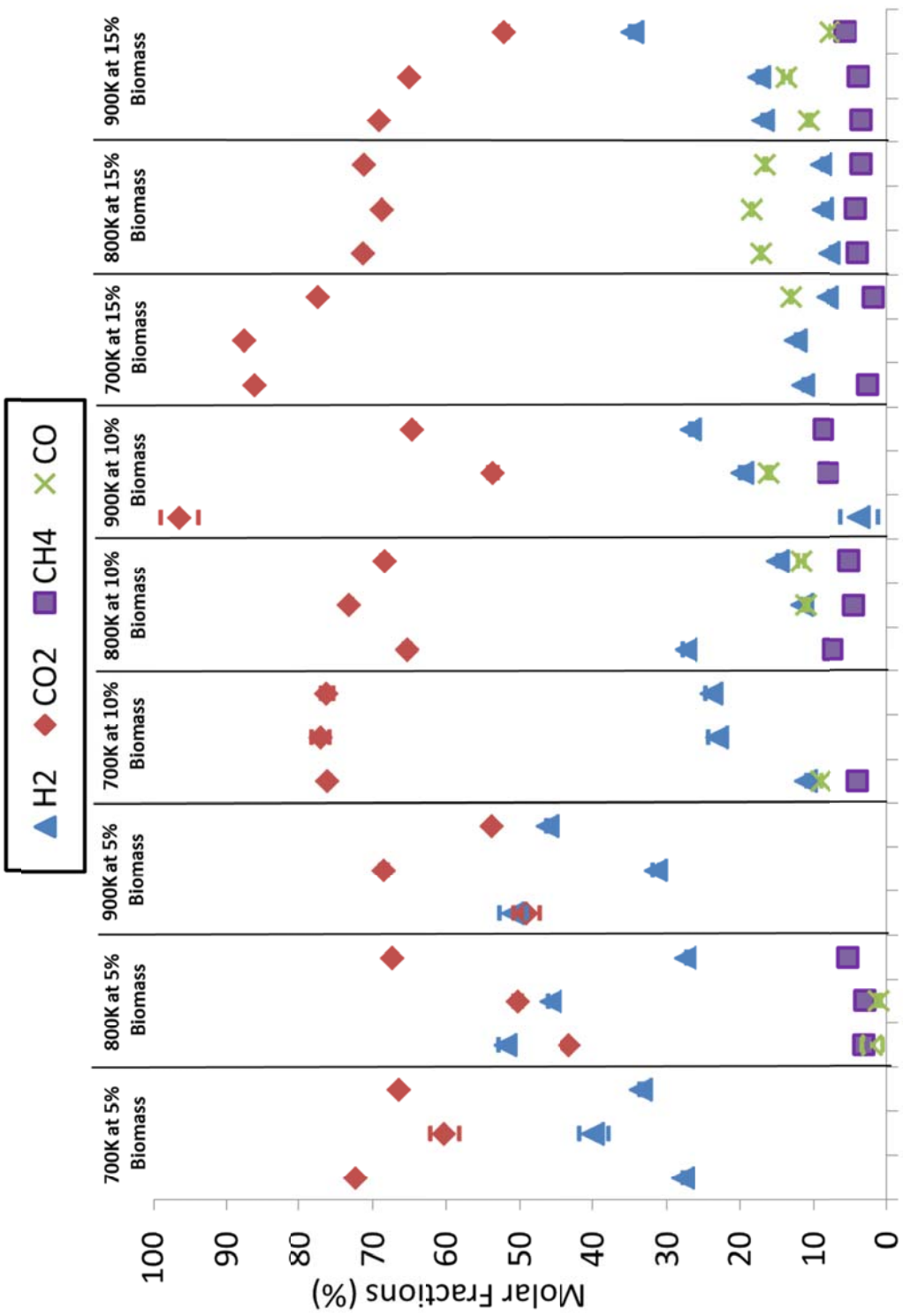

Figure 4.3.2 (A): Syngas composition for all individual process runs, with each set of triplicate measurements demarked by vertical lines. Error bars indicate variations in the GC replicate measurements of gas concentrations.

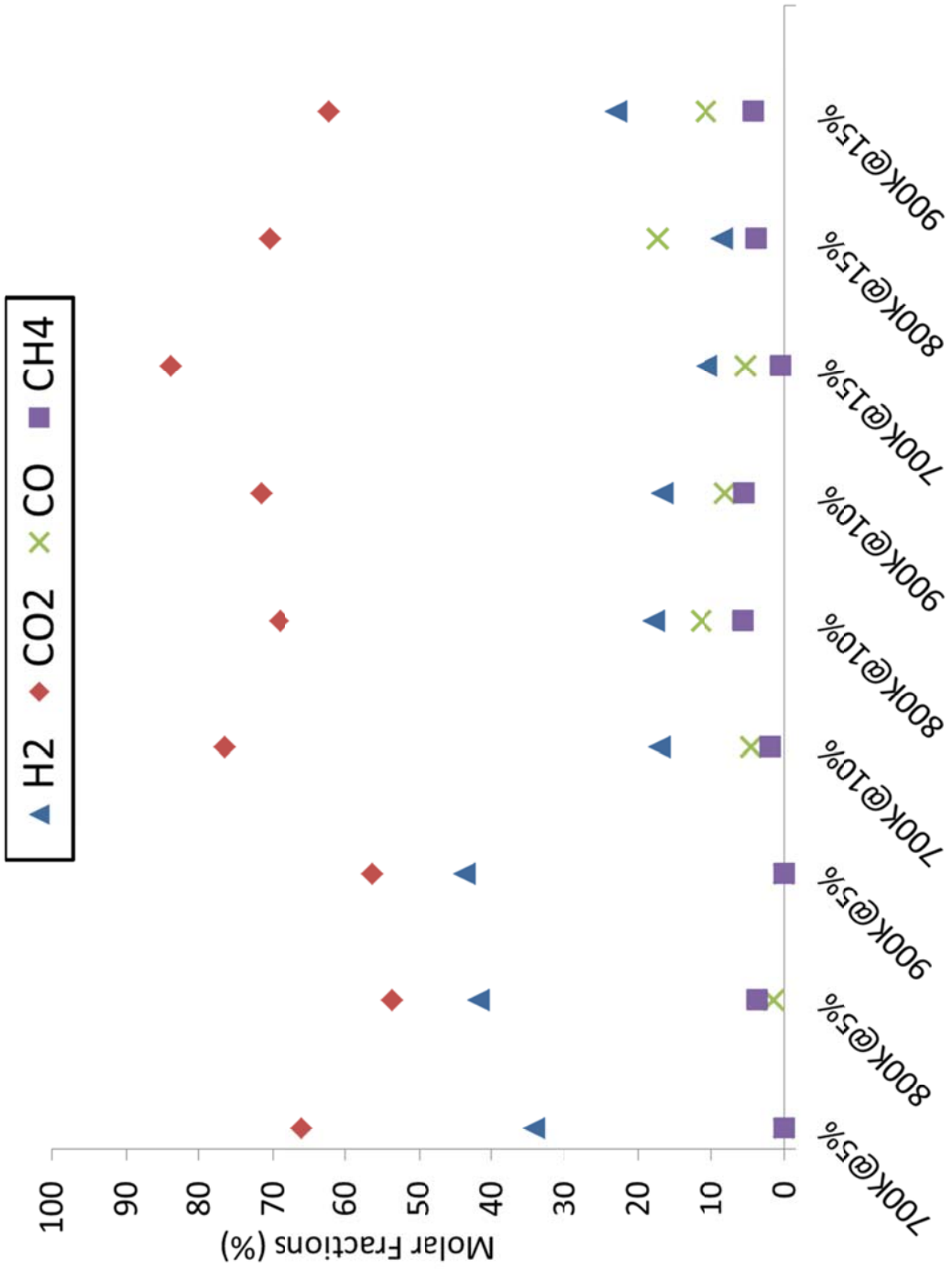

Figure 4.3.2 (B): Syngas composition for collated process runs, with each set of triplicate measurements averaged into a single data point.

Figure 4.3.3 plots the syngas composition as a function of biomass concentration at each temperature (A: 700K, B: 800K, and C: 900K). In each case, we present the average composition from the triplicate runs. An unambiguous trend is seen in the gas composition, and it is largely independent of temperature. Specifically, one sees that CO_2 production is high in all cases, and rises as the biomass concentration increases. H_2 production starts high (comparable to CO_2) and falls with increasing biomass concentration. Finally, CO production is negligible for the 5% biomass case and grows as biomass concentration increases. As we noted earlier, in all cases the conversion of solid biomass to non-condensable gases is high (nominally 95% over the temperature and biomass concentration range). Fig. 4.3.3 (A-C) shows that the fuel value of the mixture is highest at low biomass concentrations. Looking at the fuel composition for 5% biomass alone, one sees that higher temperatures favor more hydrogen production. This trend coincides with previous research [KEL07, HAO03, RES07, RES08, RES09, RES10, & YAN06]. That said, one should keep in mind this is based on the gas composition. If one takes into account that the conversion efficiency is nominally 95% for all runs the 10% and 15% biomass loadings create a larger quantity of syngas. For high hydrogen concentrations, the best gaseous fuels are made at low biomass loadings and higher temperatures. For raw heating value of the syngas, higher biomass concentrations may be favorable as the increase in net volumes of gas increase. Table 4.3.1 below denotes the nominal heating values for each of the process conditions. For scale-up purposes, higher temperature operation (where the fuel properties are best) is ideal for process heat integration throughout the plant, enabling a high energy efficiency production process.

Sample	Hydrogen (mol%)	Methane (mol%)	Carbon Monoxide (mol%)	Heating Value HHV (kJ/mol)
700@5	34.2%	0.0%	0.0%	97.6
800@5	41.7%	3.7%	1.5%	156.4
900@5	43.7%	0.0%	0.0%	124.8
700@10	17.1%	2.0%	4.5%	79.0
800@10	17.9%	5.6%	11.3%	132.8
900@10	16.7%	5.5%	8.0%	119.7
700@15	10.5%	0.6%	5.2%	50.0
800@15	8.4%	3.8%	17.3%	107.3
900@15	22.9%	4.2%	10.7%	133.6

Table 4.3.1: Molar fraction of combustible gases within the syngas for each operating parameter and associated net heating value for that mixture

The modest impact of temperature on conversion, and the strong impact of biomass concentration on syngas composition, suggests that inter- and intra-particle transport processes may be equally important to chemical kinetics. At the same time, because nearly all of the biomass converts to non-condensable gases, if thermodynamics dominated, one would expect to see the water gas shift push the gases to a nearly pure mixture of H_2 and CO_2 at all temperatures and biomass concentrations explored here. There clearly is a complex mix of transport and reaction occurring in our system.

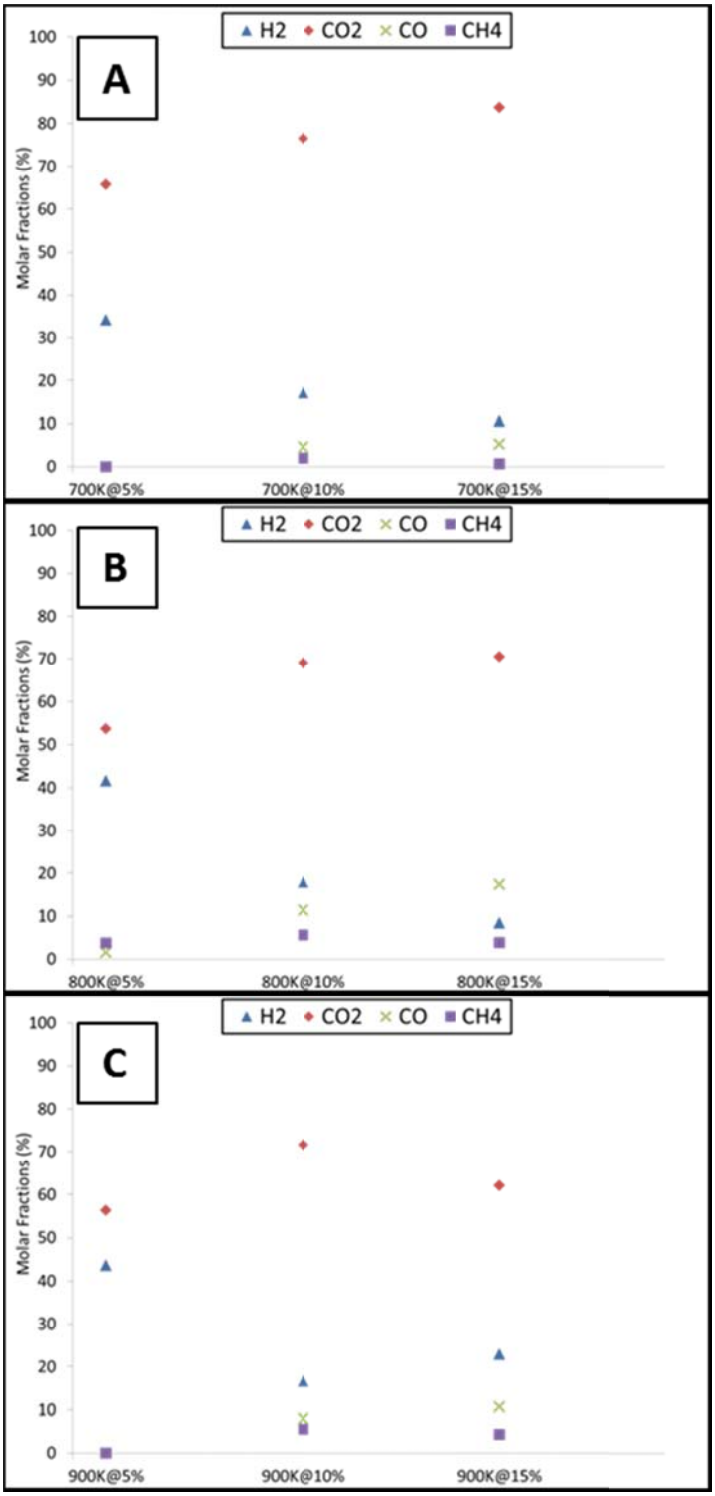

Figure 4.3.3 (A-C): (A) - Mole Fraction of Syngas Makeup at 700K across all biomass concentrations. (B) - Mole Fraction of Syngas Makeup at 800K across all biomass concentrations. (C) - Mole Fraction of Syngas Makeup at 900K across all biomass concentrations. This highlights the variability within syngas when the operating temperature is held constant and only the concentration of biomass is varied.

Not only do the data indicate coupled transport and reaction, but there is also evidence that reactions (1-9) cannot fully describe the gas stoichiometries we observe. To better illustrate this point, Figure 4.3.4 shows the average stoichiometric ratio for the product gas as a function of process variables. Here we compare H_2, CO, and CH_4 against the CO_2. The data show that the ratio of H_2:CO_2 is almost 1:1 for the 5% biomass mixture at higher temperatures, and drops below that at higher loadings and lower temperatures. The H_2:CO_2 stoichiometric ratio never exceeds 1.

We can compare the experimentally observed stoichiometry to estimates from the reaction steps that involve H_2, CO, and CO_2, namely, Steam Reforming 1 (Eq. 4), Steam Reforming 2 (Eq. 5), and water gas shift (Eq. 7). The stoichiometry of a hexose or pentose should be approximately equal to that from cellulose or hemicellulose degradation in SCW (cellulose and hemicellulose comprise approximately 70% of the mass of ponderosa pine). Simple carbohydrates have approximate stoichiometries given by x=n, y=2n, and z=n in Eqs. (4) and (5). With this assumed composition, Steam Reforming 1 produces a gas stoichiometric ratio H_2:CO of 1:1. Note that no CO_2 is produced directly in Steam Reforming 1, but if the Water Gas Shift proceeds to the right (as expected), the final gas stoichiometry ratio H_2:CO_2 is 2:1. Steam Reforming 2 directly produces a stoichiometry ratio H_2:CO_2 of 2:1. Lignin has less intrinsic molecular oxygen than carbohydrates, so the H_2:CO_2 ratio would likely exceed 2:1 for our experiments, by any of the chemical pathways represented in (1-9). The significantly lower H_2:CO_2 ratios we observe in our experiments indicate there could be an alternative oxygen source, since molecular oxygen in the biomass and water should generate a stoichiometry near 2:1. Additionally, H_2 loss from connections in the system and migration could explain part of the imbalance.

Where might this oxygen come from? The data show that the H_2:CO_2 ratio declines precipitously as biomass concentration increases, suggesting the oxygen is linked to the biomass. Given that the biomass stoichiometry is reasonably well known, and that it is not strongly oxygenated, we propose that air bubbles are trapped within the slurry. The slurry viscosity increases dramatically as the biomass concentration increases from 5% to 15% (becoming peanut butter-like). This means that bubbles entrained during blending are less likely to be released during the soaking period. In short, we believe there is partial oxidation occurring in our system via the oxygen from air. This means air entering with our real-world samples may subject the biomass to the additional chemistries.

Partial Oxidation: $$C_xH_yO_z + \frac{(x+y/2-z)}{2} O_2 \rightarrow xCO + \frac{y}{2} H_2O \quad . \qquad (10)$$

and

Combustion: $$C_xH_yO_z + (x - \frac{z}{2} + \frac{y}{4}) O_2 \rightarrow xCO_2 + \frac{y}{2} H_2O \qquad (11)$$

Partial oxidation and combustion are undesirable side reactions that produce no hydrogen until the water gas shift reaction converts any CO from (10) into H_2 and CO_2. If Eq. (10) is the dominant reaction producing CO, rather than Reforming 1, the maximum expected H_2:CO_2 ratio would be 1:1, which is close to our highest observed molar ratios. With sufficient oxygen, Eq. (11) suggests the reactor would produce neither H_2 nor CO. The molar ratios in the high biomass concentration data of Figure 8 suggests that partial oxidation and/or combustion chemisty are important for setting the final gas stoichiometry, and that Water Gas Shift has not achieved thermodynamic equilibrium in our reactor.

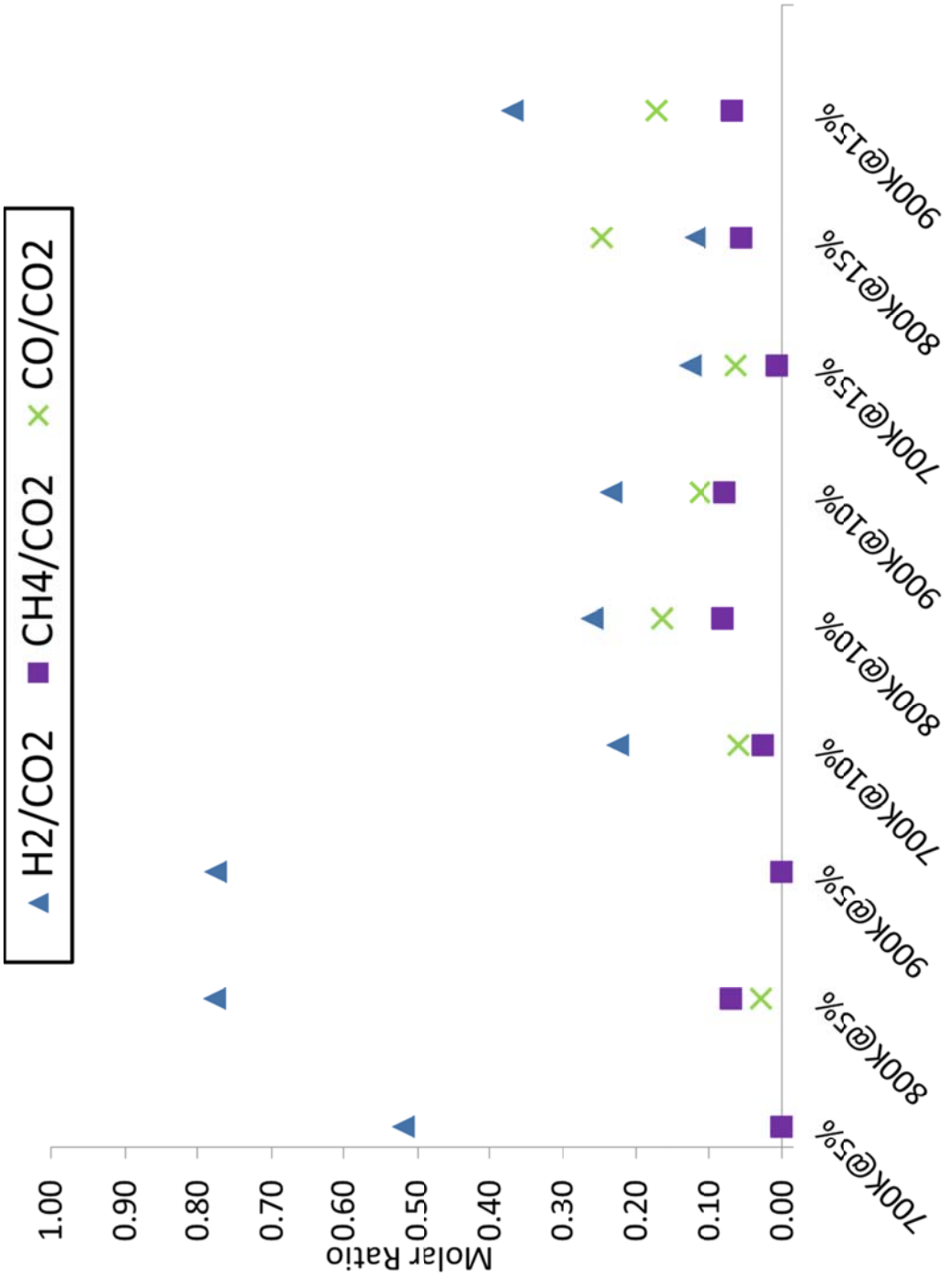

Figure 4.3.4: Mole Fraction Syngas Normalized by CO_2 Content. This figure normalizes combustible gases per CO_2 content, thereby highlighting the fuel potential of each syngas stream.

4.4 Conclusions

A new feedstock, Ponderosa Pine, has been gasified utilizing continuous feed SCW gasification. This adds to the existing body of literature and helps to demonstrate the robustness of the process. For all parameters tested conversion rates are consistently high (nominally 95%). Of significant note is the indication that using a processing rate that is much faster than that of previous research can result in higher concentrations of H_2 at lower process temperatures than previously thought [KEL07, HAO03, RES07, RES08, RES09, RES10, & YAN06]. Furthermore consistent variations in syngas composition with biomass feed concentration are shown. Under our conditions variations in biomass concentration are more important than temperature for determining product gas composition. this supports the practical goal of decreasing water concentration in the process, which reduces the energy input needed for gasification. Clear trends are shown that favors H_2 production at 5% concentrations of biomass versus 10% & 15% respectively, however all samples under all mixtures and concentrations did gasify. Additionally, it was shown that higher concentrations produce not only more syngas, but can result in a higher hearting value as well. Current reactions thought to occur in SCWG do not sufficiently describe all of the observed behavior. One possible explanation is the introduction of oxygen via air entrainment into the slurry at higher slurry concentrations.

CH 5: Evaluate Raman Spectroscopy for Use in Syngas Produced by SCW Gasification

5.1 Background

Raman spectroscopy is a measurement technique based upon the Raman effect. This effect was first discovered in 1927 and is based upon the scattering of light when it impacts a molecule [KNE99]. When this occurs, three possible types of scattering can result: Rayleigh,

Stokes, and Anti-Stokes. The latter two types of scattering result in a frequency shift in which the emitted light is either higher (Anti-Stokes), or lower (Stokes) than the original light source. A third type of scattering that can occur is inelastic scattering in which no frequency shift occurs. The inelastically scattered light (Rayleigh) (also referred to as 'Raman scattering') allows one to directly fingerprint the molecular composition of many substances. The Figure 5.1.1 below shows the characteristic vibrational energy of several bonds which are of key interest for SCW gasification: carbon monoxide, carbon dioxide, hydrogen, methane, and water molecules.

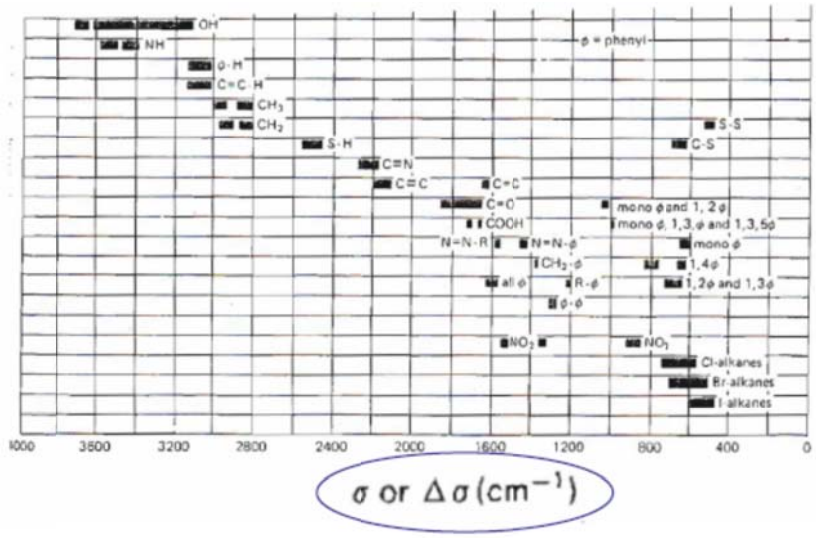

Figure 5.1.1: Group Assignment [SKO00]

Typical modern Raman spectroscopy devices use a fiber optic cable to bring monochromatic laser light to the optical probe head which is placed directly in front of the media to be measured. Because the probe is solid-state and can be constructed of high temperature materials it offers a promising means to make measurements in a SCW environment. Additionally the technique can be used on solids, liquids, and gases [KNE99]. Because SCW gasification involves all three of these states of matter simultaneously this is of significant importance.

Water can behave differently depending upon its state, which affects its behavior during Raman measurements. Typical water behaves differently than super critical water in a variety of ways. Research on super critical water itself shows the level of change that can occur pending its temperature and pressure [IKU98]. Regardless, throughout all temperature and pressure ranges Raman measurements of SCW were able to be obtained.

This author's research attempts to validate the use of Raman Spectroscopy as a tool for real time analysis of SCW gasification. Currently researchers are using offline gas chromatography to determine syngas mixtures but are unable to monitor the actual production of syngas [MAT05]. Because SCW gasification allows one to vary the composition of the syngas, having real time data gives the ability to adjust parameters to match a desired output. The importance of this for any industrial process is monumental.

5.2 Materials & Methods

Ponderosa Pine feedstock was obtained from an industrial saw mill directly from the production line. This feedstock was chosen due to its local availability and because it would allow for the testing of a real, modestly processed woody biomass resource. Samples were run with 20 mesh ground with a Wiley mill using sequential grinding. Distilled water is added to the sawdust to achieve a 5% biomass concentration (1690 grams Di water for every 90 grams of dry biomass). The biomass/water slurry was allowed to sit overnight so that the wood was saturated. This mixture was then used for our continuously fed apparatus.

For these measurements a Rxn-1 system from Kaiser Optical Systems Inc. was used. The system utilizes a 785 nm laser with a 400mW power rating. The device uses a Holoplex grating with an aperture ratio of $f/1.8$ for simultaneous collection of Raman data across the entire spectrum. Kaiser's MR series probe head is used in order to connect the laser to custom

build sapphire ball probes. The patent for these probes is owned by Brian Marquardt, the collaborator for this experiment. These probes offer a significant advantage over traditional ones in regards to focal length. Furthermore they are designed with Hastelloy connections, which are ideal for high temperature/pressure experiments.

All measurements were acquired using cosmic ray removal for clean spectra. Offline acquisitions were run for a total 30mins with 30 scans (30s each) for the blank (water) and the filtered product and 90 scans (30s each) for the unfiltered biomass slurry. Online acquisitions (super critical conditions) were a total 2mins with 30 scans (2s each) with the probe inserted mid-length along the reactor. Spectra are reported in counts per second to account for acquisition time differences and analysis was done using the Wire 2.0 software. Baselines were modeled well with cubic spline functions, thus producing flat baselines for subsequent analysis. Spectral peaks were then fitted to standard Vogt distribution profiles, and curve fit parameters were used to calculate integrated peak areas.

5.3 Results & Discussion

The first ever measurements of Ponderosa Pine during the gasification process in super critical water were obtained. This demonstrates a new and exciting possible means for real-time monitoring of super critical water gasification of actual biomass. High fluorescence was evident, however after base-lining spectra that very closely match those obtained in previous research at ambient temperatures and pressures were obtained [KAC00, MEY11, OST06]. Furthermore it was noticed that the level of fluorescence rose as samples were entered into the reactor. This offers a possible means of determining the biomass concentrations within the system. Table 5.3.1 below shows the expected peaks of cellulose and their vibrational modes at ambient temperature and pressure.

Raman Shift (cm-1)	Vibration mode
3500-3200	OH Stretch
3000-2800	CH, CH2 Stretch
1476	HCH and HOC bend
1376	HCC, HCO, and HOC bend
1334	HCC, HCO, and HOC bend
1290	HCC and HCO bend
1118	CC and CO stretch
1095	CC and CO stretch
516-379	Skeletal (CCC, COC, OCC, and OCO) bend

Table 5.3.: Expected Peaks for cellulose [OST06]

Lignin has fewer peaks with shifts occurring at 1587, 1591, 1594, 1603, and 1606 cm^{-1} [MEY11]. Hemicellulose typically shows shifts at 1026, 1034, 1041, and 1064, 1078, cm^{-1} [KAC00]. The Raman spectra for the gases expected in the syngas are as follows: Carbon Monoxide ~ 2000 cm-1 (weak), Carbon Dioxide ~ 1350 cm-1 (strong), Hydrogen ~ 4150 cm^{-1} (medium), and Methane ~ 2900 cm^{-1} (strong) [AND77, GRE03, JOU05, & MAH84]. These correspond to gas chromatography measurements made in previous research in this system with identical operating parameters. Figure 5.3.1 below shows three spectra obtained in-situ.

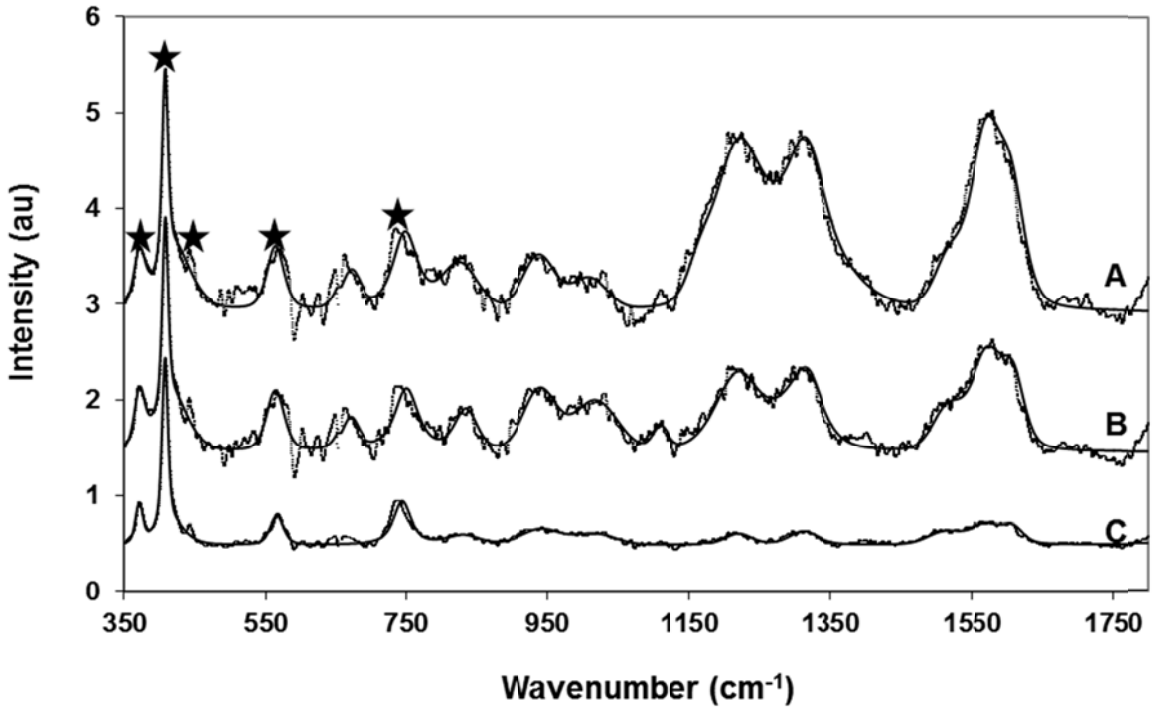

Figure 5.3.1: Raman Spectra of 5% Ponderosa Pine during gasification in Super Critical Water. Spectra A was obtained while biomass was being fed into the reactor. Spectra B and C were obtained when biomass had reached full concentration and was being gasified within the reactor at 27.7 MPa and 700 K. (Note: Starred peaks are those caused by the Sapphire probe tip)

Spectra A was obtained while the biomass slurry was being introduced into the system. Spectras B & C were obtained sequentially as biomass was pumped through the reactor during gasification. While it is obvious that the peaks for cellulose and lignin overlap those where one would expect to see the syngas, the biomass itself is easily identifiable. While it was originally hoped that it might be possible to identify the syngas products being produced the fluorescence and signal strength from the biomass simply precludes such possibility. Nonetheless we are able to monitor key aspects of the reaction.

The area of the peaks within each spectra gives key insights into the proportion of which parts of the biomass molecules are decomposing first. Peaks associated with cellulose in Spectra B (1150-1350 cm $^{-1}$) have an area of 9,400 whereas peaks associated with lignin (1500-1600 cm $^{-1}$) have an area of 9,800. Spectra A, taken at a later time during processing shows an area of 29,000 for cellulose and 19,000 for lignin. This is a strong indicator that lignin is breaking down faster inside the reactor than cellulose. Furthermore, the ratio of skeletal bonds within the cellulose (the ratios of peaks in the 950 cm^{-1} range to the 1200 cm^{-1}) change as well between Spectra A and Spectra B. A cellulose molecule is shown below in Figure 5.3.2

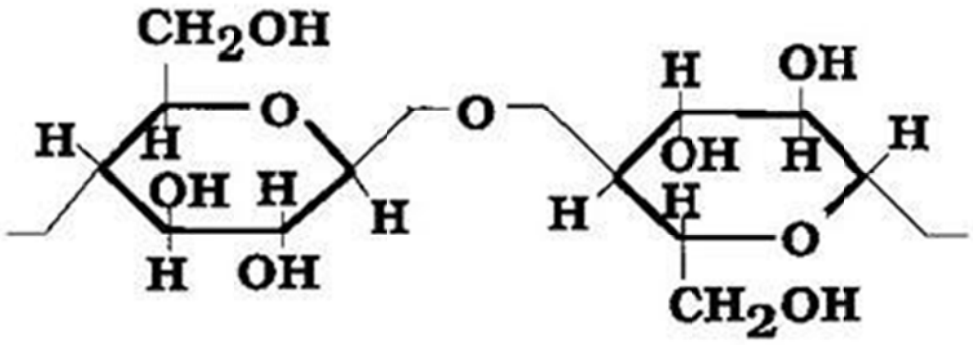

Figure 5.3.2: Cellulose molecule showing the skeletal bonds and central bonds that can be associated with peaks evident in the Raman spectra.

In order to demonstrate the amount to which the biomass slurry fluoresces in addition to providing information on it prior to being run through the reactor, spectra for the unprocessed slurry and post=processed effluent were also taken. For the sake of comparison raw spectra for the distilled water used to make the mixture was also taken. These three spectra are shown below in Figure 5.3.3 below. The biomass shows a very high fluorescence as expected and is easily distinguishable from that of the distilled water and effluent. One should note that the effluent was filtered in order to prevent any residual biomass from fluorescing and distorting reading.

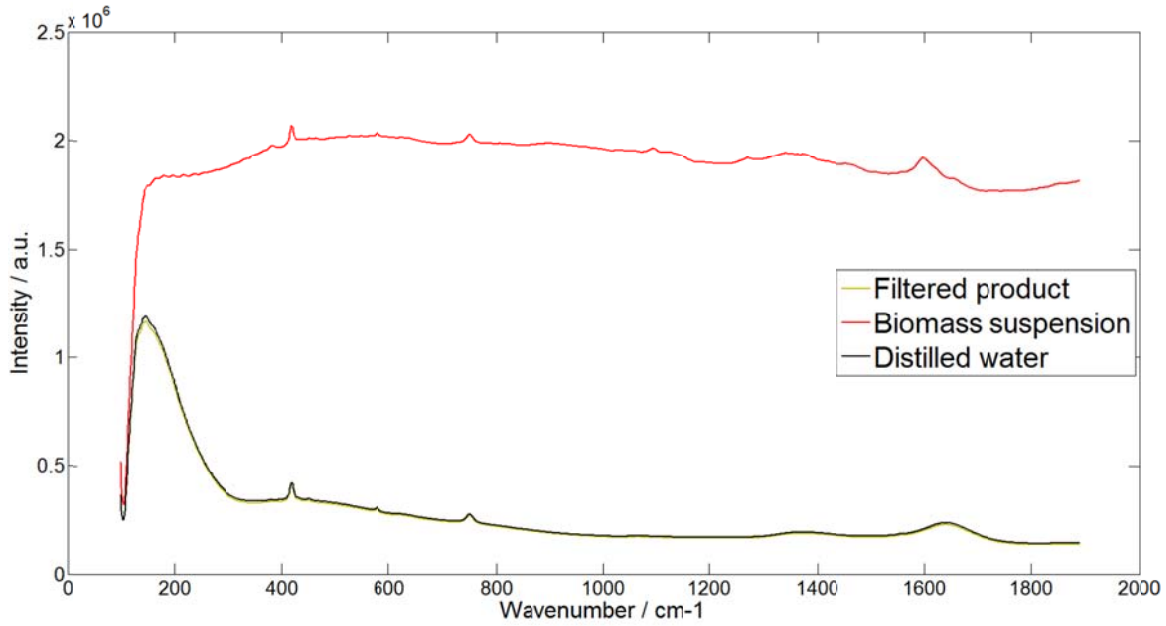

Figure 5.3.3: Raman Spectra of unprocessed 5% Ponderosa Pine, distilled water and filtered effluent post-processing of 5% Ponderosa Pine. The purpose of this set of spectra is to demonstrate the before and after spectra with DI water acting as a reference. Note that the spectra of the post-process effluent is so close to DI water as to be nearly indistinguishable.

In an effort to determine the existence of any soluble compounds within the effluent the spectra for it and the distilled water were base-lined and displayed together in Figure 5.3.4. Due to the use of a sapphire ball probe there are sharp peaks evident between 400 & 800 cm^{-1}. The remaining peaks are those of the actual distilled water and effluent. Even in the expanded view it is very difficult to discern any differences between the two spectra demonstrating that the effluent is devoid of any stray compounds cause by partial degradation of the biomass during processing. Resende, et al. provided a more comprehensive reaction network to account for the formation of nearly all dominant products from SCWG [RES07, RES08, RES09, & RES10]:

Lignin Hydrolysis $(C_{10}H_{10}O_3)_n + nH_2O \rightarrow nC_{10}H_{12}O_4$ (1)

Monomer Oligomerization	$nC_{10}H_{12}O_4 \rightarrow (C_{10}H_{10}O_3)_2 + (C_{10}H_{10}O_3)_3 + \ldots$	(2)
Monomer Decomposition:	$C_{10}H_{12}O_4 \rightarrow C_xH_yO_z$	(3)
Steam Reforming I:	$C_xH_yO_z + (x-z)H_2O \rightarrow xCO + (x-z+y/2)H_2$	(4)
Steam Reforming 2:	$C_xH_yO_z + (2x-z)H_2O \rightarrow xCO_2 + (2x-z+y/2)H_2$	(5)
Char Formation:	$C_xH_yO_z \rightarrow wC + C_{x-w}H_yO_z$	(6)
Water-gas Shift:	$CO + H_2O \rightarrow CO_2 + H_2$	(7)
Methanation:	$CO + 3H_2 \rightarrow CH_4 + H_2O$	(8)
Hydrogenation:	$CO + 2H_2 \rightarrow CH_4 + 1/2O_2$	(9)

By following this proposed reaction chemistry it can be seen that a number of products can possibly be formed. The spectra of the effluent is so close to that of the distilled water that it is nearly indistinguishable. Previous research demonstrated a nominal conversion efficiency of 95% under these parameters. Figure 5.3.5 shows the sample prior to processing and the effluent prior to being filtered. While some color is evident in the effluent, the spectra below are a strong indicator that the unconverted biomass did not undergo any chemistry changes that would have resulted in it being dissolved in the effluent.

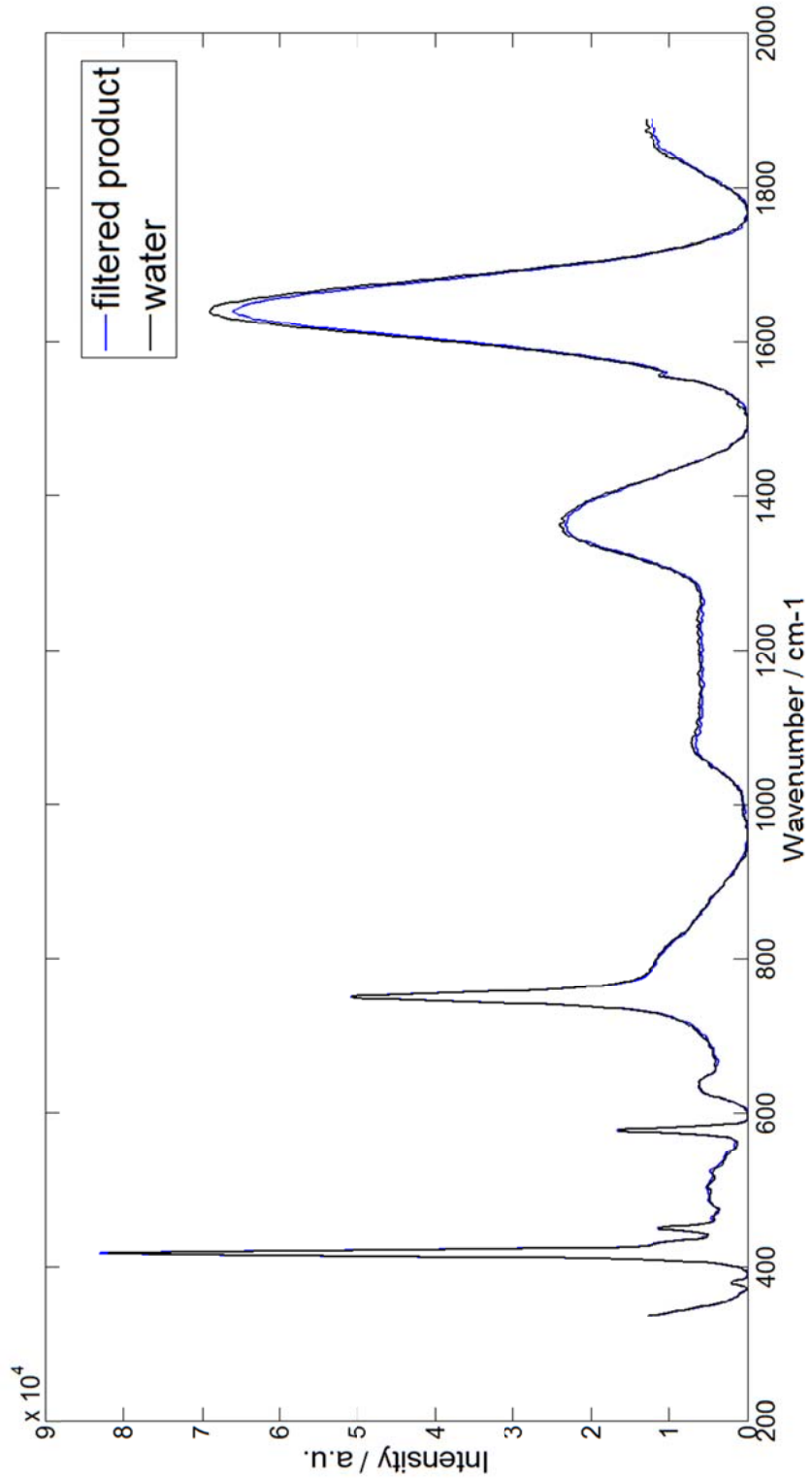

Figure 5.3.4: Raman Spectra of distilled water and filtered effluent post-processing of 5% Ponderosa Pine after base-lining. Note that all peaks are congruent and that the effluent does not have any peaks that are not evident in the DI water. This shows that no compounds are evident in the effluent.

Figure 5.3.5: Example of the liquid solution left over after processing. The effluent samples are arranged so that the left sample is unprocessed biomass slurry whereas the one on the right is post process effluent.

5.5 Conclusions

A new and exciting means for in-situ monitoring of the gasification of biomass in super critical water has been successfully demonstrated. Thanks to an innovative ball probe design spectra within the reactor section were successfully taken. While syngas was unidentifiable due to its lower signal strength versus that of the biomass, cellulose and lignin peaks were easily identifiable. Furthermore it was noted that as biomass was introduced into reactor the levels of fluorescence increased steadily until the spectra stabilized. This offers a means by which to determine biomass concentrations within the reactor. Measurements were also taken of the biomass slurry prior to processing and the post-process effluent. This data compliments the

previous research done under these parameters in that it shows that there are no identifiable compounds appearing in the effluent.

CH6: Recommendations and Future Work

In order to increase understanding of syngas makeup and feedstock, future work should focus exploring the phenomenon causing the shift in syngas between the 5% and 10% biomass concentration levels. Additionally increasing biomass loadings beyond 15% should be explored in order to determine the minimal water concentration for gasification to still occur in continuous flow systems. This would result in a better understanding of the maximum energy efficiency that could be obtained by SCW gasification. Further experimentation where variation of syngas due to process times is explored could offer another means by which to control syngas composition.

In order to increase understanding of in-situ testing, future work should focus exploring the spectra and attempting to isolate more compounds. As this system encompasses a very complicated reaction pathway, the more understanding that can be obtained the higher its potential of large scale industrial use. Additionally increasing biomass loadings beyond 5% should be explored in order to determine if Raman Spectroscopy can be used to monitor higher biomass loadings in continuous flow systems.

Reference

ADA09	J.C. Adam (2009), Improved and more environmentally friendly charcoal production system using a low cost retort-kiln (Eco-charcoal), Renewable Energy 34 p1923-1925
AGA97	A. A. Aganda, P. W.Murray, S. Kionga-Kamau (1997), Temperature profiles in a wood packed bed heated by hot inert gases, TransIChemE Vol 75 Part A p677-684
ALO08	V. Alopaeus, H. Laavi, J. Aittamaa (2008), A dynamic model for plug flor reactore state profiles, Computers and Chemical Engineering 32 p1494-1506
AND77	G. Anderson (1977), The Raman Spectra of Carbon Dioxide in Liquid H_2O and D_2O, The Journal of Physical Chemistry vol 81 no3 p273-276
ANT00	M. Antal, S. Allen, X. Dai, B. Shimizu, M. Tam, M. Gronlin (2000), Attainment of the theoretical yield of carbon from biomass, Industrial & Engineering Chemistry Research 39 p4024-4031.
ANT03	M. Antal (2003) The art, science, and technology of charcoal production, Industrial & Engineering Chemistry Research 42 p1619-1640
BEES	BEES
CAR05	Matteo Carpentieri, Andrea Corti, Lidia Lombardi (2005), Life cycle assessment (LCA) of an integrated biomass gasification combined cycle (IBGCC) with CO2 removal Energy Conversion and Management 46 p1790–1808
CHA08	A. Chaloulakou, I. Mavroidis, I. Gavriil (2008), Compliance with the annual NO_2 air quality standards in Athens. Required NO_x levels and expected health implications. Atmospheric Environment 42 p454-465
CHI93	Emmanuel N. Chidumayo (1993), Zambian charcoal production, Energy Policy p586-597
COR04	Andrea Corti, Lidia Lombardi (2004), Biomass integrated gasification combined cycle with reduced CO2 emissions: Performance analysis and life cycle assessment (LCA) Energy 29 p2109–2124
CUN08	J. Cundiff, R. Grisso (2008) Containerized handling to minimize hauling cost of herbaceous biomass, Biomass and Bioenergy 32 p308-313
DAV04	R.R. Davda, J.A. Dumesic (2004), Renewable hydrogen by aqueous-phase reforming of glucose Chemical Communications no1 p36-37
DIB07	Colomba Di Blasi, Carmen Brancaa, Antonio Galganoa, Dietrich Meierb, Ina Brodzinskib (2007), Supercritical gasification of wastewater from updraft wood gasifiers, Biomass and Bioenergy 31 p802–811
DOW07	N. Dowling (2007), Mechanical Behavior of Materials Engineering Methods for Deformation, Fracture, and Fatigue, Upper Saddle River, NJ: Prentice Hall
EIA12	US Energy Information Administration: http://tonto.eia.doe.gov/energyexplained/index.cfm?page=oil_home#tab2
ERI08	L. Eriksson (2008) Comparative analyses of forest fuels in a life cycle perspective with a focus on transport systems, Resources Conservation and Recycling 52 p 1190-1197
FAR96	Farone, W. A and J. E. Cuzens (1996). Method of Producing Sugars Using Strong

	Acid Hydrolysis of Cellulosic and Hemicellulosic Materials. U.S.P Office **5,562,777**
FOG05	H. Fogler (2005), Elements of Chemical Reaction Engineering 4th edition, , Upper Saddle River, NJ: Prentice Hall
FOO87	Food and Agriculture Organization of the United Nations, Simple Technologies for Charcoal Making, 1987, available at http://www.fao.org/docrep/X5328e/x5328e00.HTM.
FOR00	Goran Forsberg (2000), Biomass energy transport Analysis of bioenergy transport chains using life cycle inventory method, Biomass and Bioenergy 19 p17-30
GOR00	V. Gorokhov, L. Manfredo, J. Ratafia-Brown, M. Ramezan, G. Stiegel (2000), Life Cycle Assessment of Gasification-Based Power Cycles, Proceedings of 2000 International Joint Power Generation Conference July 23-26
GRE03	E. Gregoryanz, A. Goncharov, K. Matsuishi, H. Mao, R. Hemley (2003) Raman Spectroscopy of Hot Dense Hydrogen, Physical Review Letters of The American Physical Society vol 90 number 17 p1757011-1757014
GREET	Greet Data Base
GOY06	H.B. Goyal, Diptendu Seal, R.C. Saxena (2006) Bio-fuels from thermochemical conversion of renewable resources: A review, Renewable and Sustainable Energy Reviews
GUO07	L.J. Guo, Y.J. Lu, X.M. Zhang, C.M. Ji, Y. Guan, A.X. Pei (2007), Hydrogen production by biomass gasification in supercritical water: A systematic experimental and analytical study, Catalysis Today vol129 issues 3-4 p275-286
HAM05	C. Hamelinck, R. Suurs, A. Faaji (2005), International bioenergy transport costs and energy balance, Biomass and Bioenergy 29 p114-134
HAS07	R. Hashaikeh, Z. Fang, I. Butler, J. Hawari, J. Kozinski (2007) Hydrothermal dissolution of willow in hot compressed water as a model for biomass conversion, Fuel 86 p1614-1622
HAO03	X.H. Hao, L.J. Guo, X. Mao, X.M. Zhang, X.J. Chen (2003), Hydrogen production from glucose used as a model compound of biomass gasified in supercritical water, International Journal of Hydrogen Energy 28 p55-64
HEI02	R. Heijungs, S. Suh (2002), The computational structure of life cycle assessment. Kluwer Academic Publishers. Dordrecht, The Netherlands
HES09	P. Hessburg & group [Personal Communction] July, 2009
IPCC07	Forster, P., V. Ramaswamy, P. Artaxo, T. Berntsen, R. Betts, D.W. Fahey, J. Haywood, J. Lean, D.C. Lowe, G. Myhre, J. Nganga, R. Prinn, G. Raga, M. Schulz and R. Van Dorland, 2007: Changes in Atmospheric Constituents and in Radiative Forcing. In: Climate Change 2007: The Physical Science Basis. Contribution of Working Group I to the Fourth Assessment Report of the Intergovernmental Panel on Climate Change [Solomon, S., D. Qin, M. Manning, Z. Chen, M. Marquis, K.B. Averyt, M.Tignor and H.L. Miller (eds.)]. Cambridge University Press, Cambridge, United Kingdom and New York, NY, USA.
JEN08	Econ Calculator Gasifier by Professor Bryan Jenkins, UCDAVIS. http://faculty.engineering.ucdavis.edu/jenkins/CBC/Calculator/EconModules/EconCalculator_Gasifier.xls
JOU05	E. Jourdanneau, F. Chaussard, R. Saint-Loup, T. Gabard, H. Berger (2005) The

	methane Raman spectrum from 1200 to 5500 cm^{-1}: A first step toward temperature diagnostic using methane as a probe molecule in combustion systems, Journal of Molecular Spectroscopy 233 p219-230
IKU98	Y. Ikushima, K. Hatakeda, N. Saito, M. Arai (1998) An in situ Raman spectroscopy study of subcritical and supercritical water: The peculiarity of hydrogen bonding near the critical point, Journal of Chemical Physics vol 108 no 14 p5855-5860
KAM08	M. Kampa, E. Castanas (2008), Human health effects of air pollution. Environmental Pollution 15 p362-367
KAN93	J. B. Kandpal, R. C. Maheshwari (1993), A decentralized approach for biocoal production in a mud kiln, Bioresource Technology 43 p99-102
KEL07	Tau Len Kelly-Yong, Keat Teong Lee, Abdul Rahman Mohamed (2007), Potential of hydrogen from oil palm biomass as a source of renewable energy worldwide, Energy Policy 35 p5692–5701
KNE99	K. Kneipp, H. Kneipp, I. Itzkan, R. Dasari, M. Feld (1999) Ultrasensitive Chemical Analysis by Raman Spectroscopy, Chem Rev 99 p2957-2975
KRI04	P. Kritzer (2004), Corrosion in high-temperature and supercritical water and aqueous solutions: a review, Journal of Supercritical Fluids 29 p1-29
KRU04	A. Kruse, T. Henningsen, A. Sinag, J. Pfeiffer (2004), Biomass gasification in supercritical water: Influence of the dry matter content and the formation of phenols, Ind Eng Chem Res 43 p502-508
KRU08	A. Kruse (2008), Supercritical water gasification, Biofuels Bioproducts & Biorefining 2 p415-437
KRU09	A. Kruse (2009), Hydrothermal biomass gasification, The Journal of Supercritical Fluids 47 p391-399
LEH06	Johannes Lehmann, John Gaunt, Marco Rondon (2006), BIO-CHAR SEQUESTRATION IN TERRESTRIAL ECOSYSTEMS – A REVIEW, Mitigation and Adaptation Strategies for Global Change 11 p403–427
LIN06	Jeng-Chyan Muti Lin (2006), Development of a high yield and low cycle time biomass char production system, Fuel Processing Technology 87 p487-495
LIN09	Yu-Jen Lin, Gwo-Shyong Hwang (2009), Charcoal from biomass residues of a Cryptomeria plantation and analysis of its carbon fixation benefit in Taiwan, Biomass and Bioenergy 33 p1289-1294
LOM03	Lidia Lombardi (2003), Life cycle assessment comparison of technical solutions for CO2 emissions reduction in power generation, Energy Conversion and Management 44 p93–108
LU06	Y.J. Lu, L.J. Guo, C.M. Ji, X.M. Zhang, X.H. Hao, Q.H. Yan (2006), Hydrogen Production by biomass gasification in supercritical water: a parametric study, International Journal of Hydrogen Energy31 p822-831
LU07	Youjun Lu, Liejin Guo, Ximin Zhang, Qiuhui Yan (2007), Thermodynamic modeling and analysis of biomass gasification for hydrogen production in supercritical water, Chemical Engineering Journal 131 p233–244
MAH84	M. Mahoney, M. Howard, R. Cooney (1984), Raman Spectra of Carbon Monoxide

	Adsorbed on Silver Electrodes, Journal Electroanalytical Chemistry 161 p163-167
MAN97	M. Mann, P. Spath (1997), Life Cycle Assessment of a Biomass Gasification Combined-Cycle System
MAT05	Y. Matsumura, T. Minowa, B. Potic (2005), Biomass in near-and supercritical water: Status and prospects, Biomass and Bioenergy vol 29 issue4 p269-29
MCE00	K. McElhaney (2000), An analysis of check valve performance characteristics based on valve design, Nuclear Engineering and Design 197 p169-182
MUY99	M.S. Muylaert, J. Sala, M. Freitas (1999), The charcoal's production in Brazil — process efficiency and environmental effects, Renewable Energy 16 p1037-1040
NAT05	National Renewable Energy Laboratory (2005), Minnesota Biomass - Hydrogen and Electricity Generation Potential.
PER05	Perlack, R.D., L.L. Wright, A.F. Turhollow, R.L. Graham, B.J. Stokes, D.C. Erbach (2005) Biomass as Feedstock for a Bioenergy and Bioproducts Industry: The Technical Feasibility of a Billion-Ton Annual Supply, U.S. Department of Energy and U.S. Department of Agriculture, DOE/GO-102005-2135 and ORNL/TM-2005/66, Available at http://www1.eere.energy.gov/biomass/pdfs/final_billionton_vision_report2.pdf
PET08	D. Petrolia (2008) Economics of harvesting and transporting corn stover for conversion to fuel ethanol: A case study for Minnesota, Biomass and Bioenergy 32 p603-612
POL07	B. Polagye, K. Hodgson, P. Malte (2007), Economic analysis of bio-energy options using thinnings from overstocked forests, Biomass and Bioenergy 31 p105-125
RAF99	Angelantonio Rafaschieri, Mario Rapaccini, Giampaolo Manfrida (1999), Life Cycle Assessment of electricity production from poplar energy crops compared with conventional fossil fuels, Energy Conversion & Management 40 p1477-1493
REI03	L. Reijnders, M.A.J. Huijbregts (2003), Choices in calculating life cycle emissions of carbon containing gases associated with forest derived biofuels, Journal of Cleaner Production 11 p527–532
RES07	F. Resende, M. Neff, P. Savage (2007), Noncatalytic Gasification of Cellulose in Supercritical Water, Energy & Fuels 21 p3637-3643
RES08	F. Resende, S. Fraley M. Berger, P. Savage (2008), Noncatalytic Gasification of Lignin in Supercritical Water, Energy & Fuels 22 p1328-1334
RES09	F. Resende, P. Savage (2009), Expanded and Updated Results for Supercritical Water Gasification of Cellulose and Lignin in Metal-Free Reactors, Energy & Fuels 22 p6213-6221
RES10	F. Resende, P. Savage (2010), Effects of Metals on Supercritical Water Gasificiation of Cellulose and Lignin, Ind. Eng. Chem. Res 49 p2694-2700
RIB93	Jesse C. Ribot (1993), Forestry policy and charcoal production in Senegal, Energy Policy p559-585
RIG08	S. Rignon [Personal Communction] October 17, 2008
SCH98	Y. Schenkel, P. Bertaux, S. Vanwijnbserghet, J. Carre (1998), An evaluation of the mound kiln Carbonization Technique, Biomass and Bioenergy Vol 14 Nos 5/6 p505-

	516
SEA07	E.Searcy, P. Flynn, E. Ghafoori, A. Kumar (2007), The Relative Cost of Biomass Energy Transport, Applied Biochemistry and Biotechnology Vol136 p639-652
SEA08	T. Searchinger, R. Heimlich, R. Houghton, F. Dong, A. Elobeid, J. Fabiosa, S. Tokgoz, D. Hayes, T. Yu (2008), Use of U.S. Croplands for Biofuels Increases Greenhouse Gases Through Emissions from Land-Use Change, Science 29, vol 319, no 5867, p1238-1240
SHA03	J.W. Shabaker, G.W. Huber, R. R. Davada, R. D. Cortright, and J. A. Dumesic (2003), Aqueous-phase reforming of ethylene glycol over supported platinum catalysts, Catalysis Letters, vol. 88, no.1-2 p1–8
SHA92	N. Shah, P. Girard, C. Mezerette, A. M. Vergnet (1992), Wood to Charcoal conversion in a partial-combustion kiln: an experimental study to understand and upgrade the process, Fuel Vol 71 p955-962
SHI01	J. Shigley, C. Mischke (2001), Mechanical Engineering Design, New York, NY: McGraw Hill
SKO00	D. Skoog, D. West, F. Holler, S. Crouch (2000), Analytical Chemistry: An Introduction, Belmont, CA: Brooks/Cole
SMI09	R. Smith, Z. Fang (2009) Techniques, applications and future prospects of diamond anvil cells for studying supercritical water systems, The Journal of Supercritical Fluids 47 p431-446
SOR12	S. Sorrell, J. Speirs, R. Bentley, R. Miller, E. Thompson (2012) Shaping the global oil peak: A review of the evidence on the field sizes, reserve growth, decline rates and depletion rates. Energy 37 p709-724
STI02	D.M. Stieb, S. Judek, R.T. Burnett (2002), Meta-analysis of time-series studies of air pollution and mortality: effects of gases and particles and the influence of cause of death, age and season. Journal of the Air & Waste Management Association 52 p470–484
SYR06	C. Syred, A. J. Griffiths, N. Syred, D. Beedie, D. James (2006), A Clean, efficient system for producing charcoal, heat, and power, Fuel 85 p1566-1578
USDB	US Data Base
WAN08	L. Wang, C. Weller, D. Jones, M. Hanna (2008), Contemporary issues in thermal gasification of biomass and its application to electricity and fuel production, Biomass and Bioenergy 32 p573-581
WIK11	Wikipedia: Plug flow reactor modeling, http://en.wikipedia.org/wiki/Plug_flow_reactor_model
XU96	X. Xu, Y. Matsumura, J. Stenberg, J. Antal (1996), Carbon-catalyzed gasification of organic feedstocks in supercritical water, Ind Eng Chem Res 35(8) p2522-2530
YAN06	Qiuhui Yan, Liejin Guo, Youjun Lu (2006), Thermodynamic analysis of hydrogen production from biomass gasification in supercritical water, Energy Conversion and Management 47 p1515–1528
YAN07	Jale Yanik , Steve Ebale, Andrea Kruse , Mehmet Saglam, Mithat Yu¨ ksel (2007), Biomass gasification in supercritical water: Part 1. Effect of the nature of biomass, Fuel 86 p2410–2415

ZEL08	R Zelm, M Huijbregts, H. Hollander, H. Jaarsveld, J. Sauter, H. Wijnen, D Meent (2008), European characterization factors for human health damage of PM_{10} and ozone in life cycle impact assessment. Atmospheric Environment 42 p441-453

Appendix

7.1 Other work/projects accomplished during Phd

- Construction of Fuel Cell Test Stand
- Fuel Cell Class Winter 2008
- Fuel Cell Class Spring 2008
- USAF Biofuels Project
- CPAC Proposal ($5,000)
- Environmental Innovation Challenge 2010 (2nd place - $5,000)
- Environmental Innovation Challenge 2011 (3rd place - $2,500)
- Foster School of Business Competition (Sweet 16)
- Jone's Milestone Competition 2011 ($15,000)
- Establishment of Carbon Cultures (C Corp Founded 2012)
- Innovation Showcase 2012
- IGERT Student/TA
- Shop Master Mechanical Engineering
- Engineers Without Borders
- Jackson School Guatemala Project
- US NCAGS Liaison South Korea

7.2 Pyrolysis/Kilns

Aside from gasification, pyrolysis is another possible technique for converting biomass to a denser, more useable product. Pyrolysis is a thermally driven process wherein the existing wood structure is broken into a number of possible products. The process is performed in an oxygen limited environment and produces gases, liquids, and/or solids depending on the

temperature and process times involved. Slow, fast, and flash pyrolysis are three typical classifications with temperatures ranging from 300-1000^{o} C [GOY06 & LIN09]. Of the three, slow pyrolysis is the most suited for the production of solids.

The solid produced from slow pyrolysis, referred to as biochar, char, and/or charcoal has a number of uses and has been produced for millennia [SYR06]. Currently, uses for biochar range from soil amendments, to refining steel, to use as a fuel [CHI93, LIN09, MUY99]. Aside from altering biomass to a more useable product, slow pyrolysis offers the additional advantages of increasing energy density and reducing water [SHA92] in the resulting product. These combined aspects form a very promising solution to the multifaceted problem of removing biomass from the forest whilst overcoming the issue of transportation costs.

The method of production techniques vary but can be broken into categories along a few basic kiln types. Each of these kilns has a variety of advantages in addition to a number of disadvantages. While it might seem counterintuitive, the majority of kilns utilize technology that is hundreds if not thousands of years old [SEI08]. The efficiencies of these kilns can be as low as 8% [SEI08]. Further complicating the issue is that traditional kiln technology actually causes more pollution than open burning of the wood [ADA09]. This is due to the release of low molecular weight hydrocarbons that are unburned during the process. It is estimated that Kenya and Zambia alone pollute over 10.7 billion m^3 of air each year from the making of charcoal [ADA09]. When one looks at the total number of countries throughout the world that make char the numbers can be astounding. Industrial kilns offer a reprieve from the issue of conversion efficiency but usually at an increased transportation cost since industrial kilns are usually not located at the site where the biomass is generated. The cost of having to transport the biomass greater distances can be cost prohibitive.

Having the kiln in close proximity to the biomass significantly aids in reducing transportation issues [SEI08]. The two traditional types of kilns used in this way are pit and earth-mound kilns both of which are depicted in Figure 7.2.1. Pit Kilns are arguably the simplest and oldest type of kiln. These are formed by digging a pit with a sloping bottom which is then filled with carefully sized and stacked wood. A small dead space is left at one and then the pit is filled over with grass and dirt. Ventilation is controlled via poking air holes into the top. Above ground versions of these kilns referred to earth mound kilns offer a slight improvement in efficiency [SEI08]. These are constructed by first stacking the wood and then covering the pile with dirt. Layers of grass are sometimes used in order to aid with igniting the material. A series of holes is the placed through the mound which are closed as the process progresses, thereby allowing for air control. As pyrolysis continues the mounds are compacted down until finally the fire is extinguished after several days of smoldering.

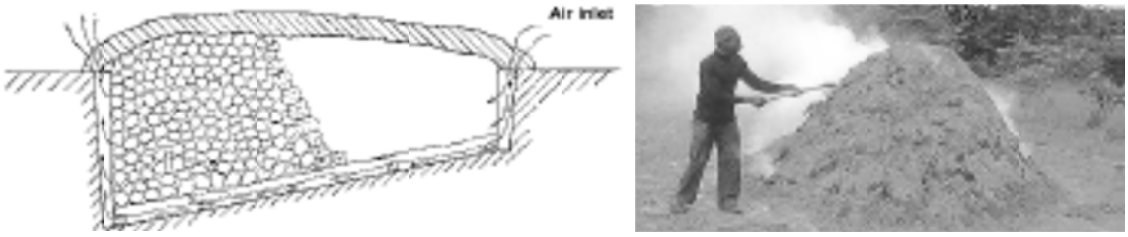

Figure 7.2.1: Pit & Earth-mound Kilns [SEI08]

Mud kilns offer further improvements over the earth-mound kiln [KAN92 & LIN09]. These are made by creating a form (often a group of logs bound together) which is then covered with mud or clay depicted in Figure 7.2.2. Fuel intakes, air intakes, and exhaust holes are created. The entire system is allowed to harden forming a rigid structure. Chimney effects can boost efficiencies up to 30% compared to the 8-20% achieved with pit and earth-mound kilns [LIN09 & SEI08]. While this boost in efficiency is of obvious benefit, the increase in labor required to produce this type of kiln means that it is typically made in a centralized location and

the biomass is brought to it. The end result is an increase in transportation costs/infrastructure. A Casamance Kiln is a compromise between an earth-mound kiln and a mud kiln where a chimney is added in effort to improve system efficiency [SEI08].

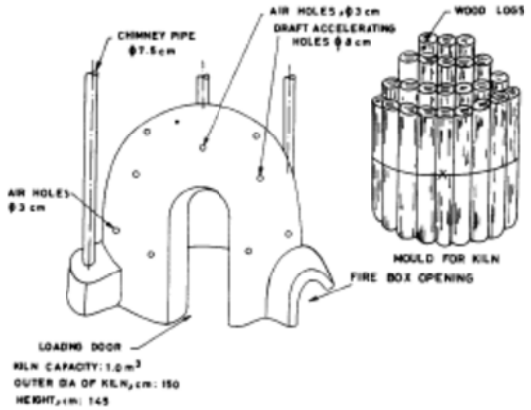

Figure 7.2.2: Mud Kiln [KAN93]

The search for ever more efficient kilns led to the creation of kilns constructed of brick and/or steel. Representations of both of these types are depicted in Figure 7.2.3 below. A large variety of these have been created with designs typically taking advantage of geometries and insulation qualities these materials respectively afford. While increases in efficiency are gained and process times reduced these have much higher associated costs and are usually located some distance from biomass which has to be transported to them [FOO87 & SEI08]. Modern industrial kilns offer the highest levels of efficiency but also are the furthest removed from the biomass source. An example of typical advancements is the Schwartz kiln, where hot gases from an external incinerator are channeled into the pyrolyzation chamber. Nearly all of the modern designs incorporate retort technology where hot gases from the pyrolyzed material is burned resulting in a higher thermal efficiency and reduced emissions [ADA09]. Sadly the tradeoff in transport distances can result in an unviable economic situation making these technologies an unsuitable option for dispersed resources.

Figure 7.2.3: Brick & Steel Kilns [SEI08]

7.3 Design & Build Mobile Pyrolysis System

As shown above, traditional kilns are typically fixed installations, most of which suffer from high levels of pollution and low levels of efficiency. The UW Bioenergy IGERT was able to test a new concept in kiln design that is both mobile and seeks to reduce emissions while improving conversion efficiency. This was a direct result of the research by UW Bioenergy IGERT projects showing that transportation costs were prohibitively high for utilizing the majority of woody biomass available within the Pacific Northwest as an energy source.

In order to achieve pyrolysis it is necessary to generate heat and control oxygen. The design concept utilized by the UW Bioenergy IGERT was to do so with a flexible membrane that was low enough in weight to be transportable. The first edition of this concept was a simple ceramic blanket draped over the pile to be pyrolyzed. It was discovered that this material was both too permeable and fragile to perform correctly. Further design resulted in laminating the ceramic core with wire mesh in order to provide a measure of durability in addition to adding mechanical strength. While this went a considerable way in improving mechanical wear, oxygen control was still less than favorable. A variety of geometries were also discussed and tested.

In an effort to improve the thermal efficiency of the system the ceramic weave was replaced with a thicker ceramic mat, reducing the outer blanket temperature to approximately 50^{o} C. This also offered safety improvements by insuring that nearby combustible materials

were not ignited. A metal laminate layer was also added to reduce the permeability of the blanket. Surface to volume ratios were improved by adding structure to the blanket in addition to attempting to provide a more consistent combustion. The size of the blanket was also increased in an effort to test the scalability and make experiments more representative of actual forest residue piles.

The end result is a modular portable kiln. Key features of the kiln are its light weight and predictable chamber geometry, modularity, the ability to manipulate air flow, and to fold it for transport. While it is hoped that this can offer a means to overcome the cost associated with utilizing forest biomass, a number of important parameters for the blanket kiln have yet to be determined. Nonetheless, a functional mobile kiln system (Figure 19 below) has been created and offers significant promise.

Figure 7.3.1: Carbon Cultures Mobile Kiln

7.4 Determine Conversion Efficiency of Mobile Pyrolysis System

Introduction

The mobile blanket kiln is a new technology inspired by the Bioenergy IGERT. As such a number of its operating parameters have yet to be determined. Of these, the system's conversion efficiency is one of the most important. This parameter plays a key role in the environmental impact and financial potential of the technology. Key parameters required in the determination of this parameter are the mass before and after processing, the water content of the biomass and the char, and the temperature profile.

Experimental Methods

Mass balance before and after burns was determined by means of an industrial scale. The biomass will be bagged into a series of bags and weighed. After completion of the burn, biochar will be collected and weighed again. It is important for the data to be relevant, that is burns must be of a representative size and biomass type be representative as well. To date this process has been completed six with the use of Alder from a slash pile in the Pacific Research Forest and Ponderosa Pine from the Yakama reservation. For the first burn the net weight of the pre-burn biomass was 295kg. Post burn weight was 64.9kg. This biochar was allowed to air-dry for 1 month in order to ensure that minimal water residue was present and the re-weighed resulting in a mass of 55.34kg (conversion efficiency of 31%). The evaporated water was accounted for and used as a baseline for future burns. It is important to note it takes several weeks for water to fully evaporate but it is anticipated will be nominally 30% confirming the first burn's results.

Water content before and after burn is a key parameter in determining the actual conversion efficiency. Green wood nominally contains 50% water; however, wood from piles that have been exposed to the elements can become water-logged and contain more moisture.

Bone dry wood contains 8-10% water content. This variability of water content in different biomass samples means it is necessary to get a representative measure of the water content present in each batch of biomass for each burn. Due to the large size of the piles and variability of the pieces it is necessary to choose a number of random pieces. The pieces are then oven dried. The weights are monitored and as the moisture content asymptotes, it allows for calculation of the water content. There are other methods for measuring moisture content such as using a small, self-contained moisture analyzer but, due to the small sample size they can accommodate, could lead to possible errors within the data. For the conducted burn, moisture contents ranged from 42-47%. It is important to note that while biochar is hydrophobic, water can still adhere to outer surfaces resulting in erroneous results if not allowed to evaporate. Therefore, in the first experiment, in order to attempt to find the bounds for how much water actually adhered to the surface, biochar was allowed to air-dry for 1 month in order to ensure that minimal water residue was present and the re-weighed. The net change was from a post-burn weight of 64.9kg to a final mass of 55.34kg. This delta was approximately 15%. For all further burns this adjustment of 15% residual water weight was accounted for in calculations. While it would have been preferable to store and dry all samples, the volume of material prohibited such. It should be kept in mind that only fully converted biochar was counted. All pieces that were not friable were considered unconverted, resulting in a fairly conservative conversion efficiency.

The processing temperature of biomass plays a significant role in its retained mass and properties [ANT00, ANT03, & SYR05]. This variability in temperature profile can result in mass differences between burns. As such it is necessary to ensure that all burns conducted, match as closely as possible in terms of process temperature. Temperature monitoring is done via a series of k-type thermocouples in a probe configuration throughout the pile. Temperature control is achieved by varying the aperture size on a series of vents incorporated onto the

blanket kiln. By monitoring airflow it is possible to vary the temperature within the system. At 400^{o} C the stoichiometric conversions of cellulose is approximated by $C_6H_{10}O_5 \rightarrow 3.75C_{0.60}O_{0.13} + 2.88H_2O + 0.5CO_2 + 0.25CO + C_{1.5}H_{1.25}O_{0.38}$ [ANT03].

In order to obtain a better grasp of the properties of the biochar a thermogravimetric analysis (TGA) was performed on experiments 4-6. Thermogravimetric analysis offers a simple but effective means by which to characterize some of the aspects of the char produced by the mobile kiln. The technique works via the use of a precision balance contained within a furnace that can be heated/cooled precisely. Furthermore, the environment can be controlled by introducing any variety of gases into the system. Types of gases can range from inert to those that allow combustion. For the purpose of the TGA, biochar was oven dried at 93^{o}C and then ground to a 40 mesh using a Wiley Mill grinder. The test procedure involved 3 steps: 1) heating biochar at a rate of 20°C/min to 110°C and holding for 5 min to determine moisture content,

2) heating from 110°C at 20°C/min to 900°C and holding for 20 min in order to determine percentage of volatiles, and finally

3) introducing oxygen to combust char and determine ash content.

This three step process was performed with biochar samples from the last 3 field experiments.

Results

The net result for the 1st burn conducted with the latest geometry system was a 31% efficiency of conversion. For that burn, the net weight of the pre-burn biomass was 295kg. Biochar was allowed to air-dry for 1 month in order to ensure that minimal water residue was present and then re-weighed resulting in a mass of 55.34kg (conversion efficiency of 31%).

Five more burns have since been conducted with two at an average temperature of 450^{o} C and three at 550^{0}C nominally. The temperature control of burns is plus or minus 50^{o} C. Five of the six experiments were maintained at plus or minus 25^{o}C. It is important to note it takes several weeks for water to fully evaporate, therefore, an adjustment in mass by 15% was used for experiments in order to account for any residual water. Furthermore, pieces that were not fully converted (i.e. not friable) were not considered in order to add in an additional margin of conservatism. Figure 7.4.1 below is an illustration of alder that was been converted to biochar during the first burn.

Figure 7.4.1: Biochar from alder produced with the mobile kiln

Burns 1, 4, 5, and 6 were conducted with alder in the Pacific Research Forest. Burns 2 & 3 were conducted at the Yakama Indian reservation utilizing Ponderosa pine. While experimenters attempted to maintain a somewhat consistent diameter of slash within each sample, average pieces ranged from 1.5-4" in diameter. De-limbing was not performed one of the goals was to make test burns as realistic as possible and minimize any preparations to the pile. Additionally, it was thought that the finer pieces of biomass might assist in the initial ignition of the pile. One should note that the height of the kiln was reduced by 2ft after Experiment 1 in order to reduce the volume to a more manageable size. A photo of that kiln (Figure 7.4.2) is shown below. This kiln was used for all further experiments.

Figure 7.4.2: Shortened Mobile Kiln

The results from the six field experiments are shown below in Table 7.4.1. Of note is that all six experimental results, with the exception of 3 and 5, are within a percent or two of each other. Experiment 5 contained a significant amount of under-processed char which was not counted; thus, the lower yield is to be expected. Experiment 3 was conducted with bailed Ponderosa pine pieces with a nearly identical diameter, therefore allowing for a more uniform process. While this was not done on purpose it does offer some insight into possible gains in efficiency by sorting of slash.

Experiment #	Net Mass (kg)	Water content	Mass biomass (kg)	Mass Biochar (kg)	Conversion
1	295.0	40.0%	177.0	55.3	31.3%
2	153.8	10.0%	138.4	54.2	33.3%
3	93.4	10.0%	84.1	43.0	43.4%
4	175.0	10.0%	157.5	62.2	33.6%
5	173.2	10.0%	155.9	43.0	23.4%
6	162.3	10.0%	146.1	55.9	32.5%

Table 7.4.1: Conversion & Mass balance data for field experiments

TGA showed very consistent results for all samples processed and demonstrates the robustness of the process. Variation in moisture was within one percent, which could easily be attributed to any residual water from the quenching process. Ash content, as expected from samples originating from a common feedstock (alder), were also consistent. Figures 7.4.3-7.4.5 show the raw TGA curves for each of the three biochar samples. These same values are presented in Table 7.4.2.

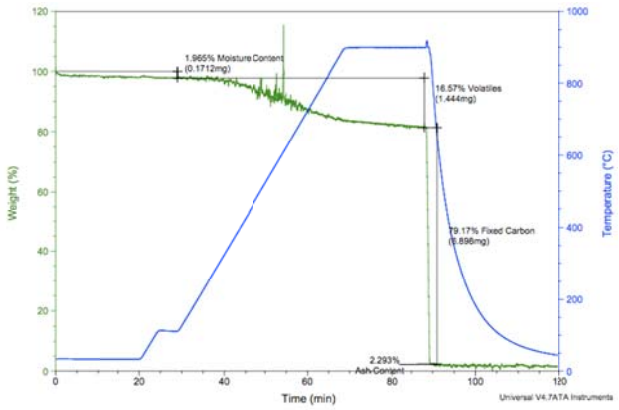

Figure 7.4.3: TGA Sample 4

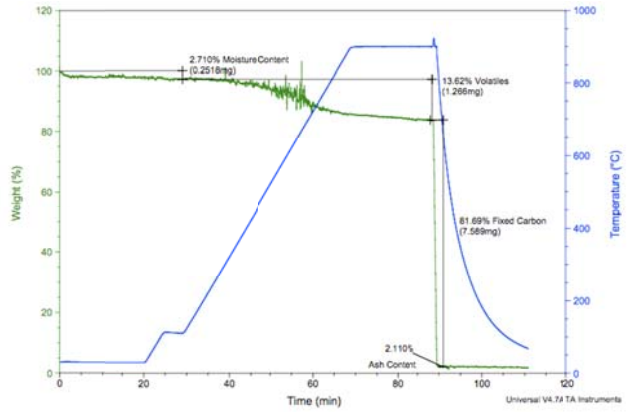

Figure 7.4.4: TGA Sample 5

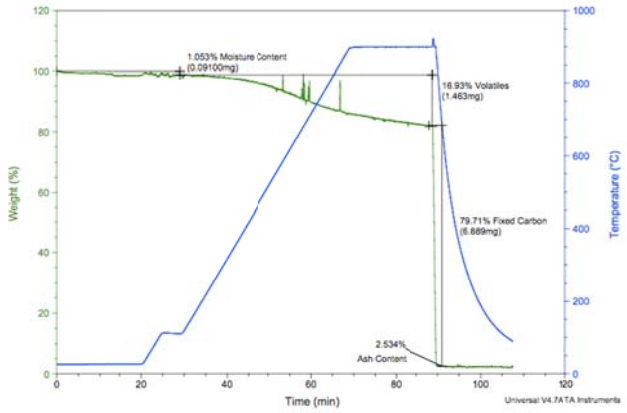

Figure 7.4.5: TGA Sample 6

Sample	Moisture Content (%)	Volatiles (%)	Fixed Carbon (%)	Ash Content (%)
4	1.97	16.6	79.2	2.29
5	2.71	13.6	81.7	2.11
6	1.05	16.9	79.7	2.53

Table 7.4.2: TGA Findings of Biochar Produced via Mobile Kiln

As a baseline, alder from the same pile was run through an identical analysis. Figure 7.4.6 and Table 7.4.3 below show the results. Of note is the much higher volatile, and much

lower fixed carbon content when compared to the aforementioned biochar samples. This is to be expected as the volatiles are oxidized through the pyrolysis process, thereby providing the energy for the reaction to occur. The fixed carbon values are approaching those obtained by a fixed bed updraft gasifier [LIN06]. Shah et al obtained statistically identical values for their process in volatiles and fixed carbon [SHA92].

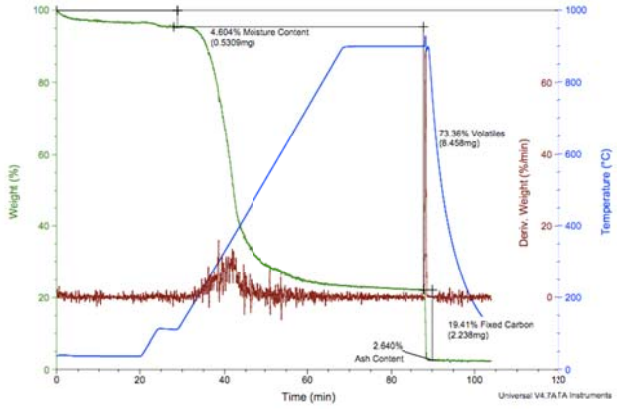

Figure 7.4.6: TGA Control Sample

Sample	Moisture Content (%)	Volatiles (%)	Fixed Carbon (%)	Ash Content (%)
Control	4.60	73.4	19.4	2.64

Table 7.4.3: TGA Oven Dried Biomass

Conclusions

One should keep in mind that a total of only six field experiments have been conducted with this technology. While all materials processed were actual forest residues of two different feedstocks processed on-site, results are amazingly consistent. Four out of six experiments produced conversion efficiencies within a few points of one another. Of the two that differed it should be noted that the experiment with the lower conversion efficiency contained a high

amount of non-converted material (due to not allowing enough cook time). Notwithstanding these two outliers, the mobile kiln has shown itself quite consistent in all measured parameters with a nominal efficiency around 30%. This far exceeds that of contemporary on-site kilns and demonstrates the effectiveness of the technology [SEI08 & KAN93].

7.5 Safety Factor Calculations

For feed tank analysis

Stainless steel 304 – matweb: http://www.matweb.com/search/DataSheet.aspx?MatID=12674

σ_{ult}=73,200psi=505MPa Kic=approx 200MPa*$m^{1/2}$

σ_{yield}=31,200psi=215MPa

CTE= 9.89 µin/in-°F (17.8 µm/m-°C) @250°C

Thermal Conductivity= 112.0 BTU-in/hr-ft²-°F (16.2 W/m-K)

σ_{yield} Verified on McMaster Carr website (supplier) as 30kpsi. Used most conservative value:

For Feed Tank Calculations:

σ_{yield} = 30,000psi

critical crack size=1/π*(Kic/σ)^2= (calculated at yield stress) =1/π*(200/215)^2=0.275m>>thickness (therefore leak before crack criteria met).

$$\sigma_{l-max} = \frac{pr_i^2}{r_o^2 - r_i^2} = \frac{5{,}000psi * 1_i^2}{1.75_o^2 - 1_i^2} = 2{,}420psi$$

$$\sigma_{t-max} = \frac{p(r_o^2 + r_i^2)}{r_o^2 - r_i^2} = \frac{5{,}000psi(1.75_o^2 + 1_i^2)}{1.75_o^2 - 1_i^2} = 9{,}850psi$$

Safety factor =$\sigma_{yield}/\sigma_{max}$=30,000/13,000= 3.05 (for maximum design operating pressure of 5,000psi=34.47MPa)

For reactor analysis

Inconel 625 – matweb: http://www.matweb.com/search/DataSheet.aspx?MatID=17402

σ_{ult}=110,000psi=760MPa @ 1200°F (650°C) Kic=approx 700MPa*$m^{1/2}$

σ_{yield}=42,100psi=290MPa @ 1200°F (650°C)

CTE= 7.11 µin/in-°F (12.8 µm/m-°C)

Thermal Conductivity= 68.0 BTU-in/hr-ft²-°F (9.80 W/m-K)

σ_{yield} verified on McMaster Carr website (supplier). Discrepancy due to testing temperature in that supplier lists a yield of 55kpsi (most conservative value used for calculations)

For Reactor Calculations:

σ_{yield}=42,100psi=290MPa @ 1200°F (650°C)

critical crack size=$1/\pi*(Kic/\sigma)^2$= (calculated at yield stress) $=1/\pi*(700/290)^2$=1.855m>>thickness (therefore leak before crack criteria met).

$\sigma_{l-max} = \frac{pr_i^2}{r_o^2 - r_i^2} = \frac{5{,}000psi * 0.125_i^2}{0.5_o^2 - 0.125_i^2}$=333 psi

$\sigma_{t-max} = \frac{p(r_o^2 + r_i^2)}{r_o^2 - r_i^2} = \frac{5{,}000psi(0.5_o^2 + 0.125_i^2)}{0.5_o^2 - 0.125_i^2}$=5,670psi

Safety factor =$\sigma_{yield}/\sigma_{max}$=42,100/5,667= 7.43 yield & 19.4 failure

---

For Check Valve Housing analysis

Stainless steel 309 – matweb: http://www.matweb.com/search/DataSheet.aspx?MatID=12724

σ_{ult}=55,100=380MPa @ 1200°F (650°C)

σ_{yield}=21,800psi=150MPa @ 1200°F (650°C)

CTE= 9.28 µin/in-°F (16.7 µm/m-°C)

Thermal Conductivity= 108.0 BTU-in/hr-ft²-°F (15.6 W/m-K)

σ_{yield} verified on McMaster Carr website (supplier). Discrepancy intentionally due to testing temperature in that supplier lists a yield of 40kpsi @ room temperature. The value at elevated testing temperature was intentionally used as the check valve housings will be in contact with biomass directly upstream of the reactor. The temperatures here will be below reactor temperatures (650°C +-50) but this was done to give an extremely conservative safety value. Of note is that the check valves will be upstream of the cooling Y coupler (guaranteeing a significantly lower temperature in the check valve housings).

For Check Valve Calculations:

σ_{yield} = 21,800psi

$\sigma_{l-max} = \frac{pr_i^2}{r_o^2 - r_i^2} = \frac{5{,}000psi * 3/8_i^2}{5/8_o^2 - 3/8_i^2}$=2,813 psi

$\sigma_{t-max} = \frac{p(r_o^2 + r_i^2)}{r_o^2 - r_i^2}$=$\frac{5{,}000psi(5/8_o^2 + 3/8_i^2)}{5/8_o^2 - 3/8_i^2}$=10,625 psi

Safety factor =$\sigma_{yield}/\sigma_{max}$=21,800/10,625= 2.05 (for maximum design operating pressure of 5,000psi=34.47MPa)

7.6 Conversion Efficiency, Flow Rate, and Mesh Size information

Sample	Flow Rate (g/s)	mesh	Conversion Efficiency	Sample	Flow Rate (g/s)	mesh	Conversion Efficiency	Sample	Flow Rate (g/s)	mesh	Conversion Efficiency
700@5	1	20	99%	700@10	3	raw		700@15	2	40	95%
700@5	1	20		700@10	3	raw		700@15	2	40	
700@5	1	20		700@10	3	40	89%	700@15	3	40	
800@5	2	20	99%	800@10	4	40	98%	800@15	5	40	91%
800@5	2	20		800@10	2	40		800@15	5	40	
800@5	2	20		800@10	3	40		800@15	4	40	
900@5	2	20		900@10	4	40	98%	900@15	4	40	
900@5	2	20		900@10	5	40		900@15	4	40	
900@5	2	20	99%	900@10	4	40		900@15	4	40	91%

Table 7.6.1: Approximate Flow Rate & Particle Size in System